

1 **Biotic Response of Plankton Communities to Middle to Late**
2 **Miocene Monsoon Wind and Nutrient Flux Changes in the**
3 **Oman Margin Upwelling Zone**

4 Gerald Auer¹, Or M. Bialik^{2,3}, Mary-Elizabeth Antoulas¹, Noam Vogt-Vincent⁴, Werner E.
5 Piller¹

6 ¹University of Graz, Department of Earth Sciences, NAWI Graz Geocenter, Heinrichstrasse 26, 8010 Graz, Austria

7 ²University of Muenster, Institute of Geology and Palaeontology, Corrensstr. 24, 48149 Münster, Germany

8 ³Dr. Moses Strauss Department of Marine Geosciences, The Leon H. Charney School of Marine Sciences,
9 University of Haifa, Carmel 31905, Israel.

10 ⁴Department of Earth Sciences, University of Oxford, Oxford, UK

11 *Correspondence to: Gerald Auer (gerald.auer@uni-graz.at) & Or M. Bialik (obialik@uni-muenster.de)*

12
13 **Keywords**

14 Indian summer monsoon, upwelling, Miocene, calcareous nannoplankton, intermediate waters, nutrient fluxes

15

16

17 **Abstract.** Understanding past dynamics of upwelling cells is an important aspect of assessing potential upwelling
18 changes in future climate change scenarios. Our present understanding of nutrient fluxes throughout the world's
19 oceans emphasizes the importance of intermediate waters transporting nutrients from the Antarctic divergence into
20 the middle and lower latitudes. These nutrient-rich waters fuel productivity within wind-driven upwelling cells in
21 all major oceans. One such upwelling system is located along the Oman Margin in the Western Arabian Sea
22 (WAS). Driven by cross-hemispherical winds, the WAS upwelling zone's intense productivity led to the formation
23 of one of the most extensive oxygen minimum zones known today.

24 In this study covering the Middle to Late Miocene at ODP Site 722, we investigate the inception of upwelling-
25 derived primary productivity. This study presents new plankton assemblage data in the context of existing model-
26 and data-based evidence constraining the tectonic and atmospheric boundary conditions for upwelling in the WAS.
27 With this research, we build upon the original planktonic foraminifer-based research by Dick Kroon in 1991 as
28 part of his research based on the Ocean Drilling Project (ODP) LEG 117.

29 We show that monsoonal winds likely sustained upwelling since the emergence of the Arabian Peninsula after the
30 Miocene Climatic Optimum (MCO) ~14.7 Ma, with fully monsoonal conditions occurring since the end of the
31 Middle Miocene Climatic Transition (MMCT) ~13 Ma. However, changing nutrient fluxes through Antarctic
32 Intermediate and sub-Antarctic Mode Waters (AAIW/SAMW) were only established after ~12 Ma. Rare
33 occurrences of diatoms frustules correspond to the maximum abundances of *Reticulofenestra haqii* and
34 *Reticulofenestra antarctica*, indicating higher upwelling-derived nutrient levels. By 11 Ma, diatom abundance
35 increases significantly, leading to alternating diatom blooms and high-nutrient-adapted nannoplankton taxa. These
36 changes in primary producers are also well reflected in geochemical proxies with increasing $\delta^{15}\text{N}_{\text{org}}$ values (> 6‰)
37 and high organic carbon accumulation. These proxies provide further independent evidence for high productivity
38 and the onset of denitrification simultaneously.

39 Our multi-proxy-based evaluation of Site 722 primary producers provides evidence for a stepwise evolution of
40 Middle to Late Miocene productivity in the western Arabian Sea for the first time. The absence of a clear
41 correlation with existing deep marine climate records suggests that local processes, such as monsoonal wind
42 conditions but crucially also hints at changing lateral nutrient transport through upwelling intermediate waters,
43 likely played an important role in modulating productivity in the western Arabian Sea. Finally, we show that using
44 a multi-proxy record provides novel insights into how plankton responded to changing nutrient conditions through
45 time in a monsoon-wind-driven upwelling zone.

46 1. Introduction

47 Within coastal upwelling zones, wind-driven Ekman transport brings nutrient-rich deep water into the photic zone
48 (Woodward et al., 1999). This process supports enhanced primary productivity in the surface ocean. This increased
49 productivity supports a large biomass across the entire food chain, reaching far afield from the core of the
50 upwelling zone. In addition, the high productivity in upwelling zones produces a significant amount of marine
51 snow (both organic and inorganic), which sinks through the water column. As the organic particulates fall, they
52 become partially remineralized, consuming oxygen and forming an oxygen-depleted zone. (Morrison et al., 1998;
53 McCreary et al., 2013) However, the flux of organic matter is so large that a significant volume of organic matter
54 reaches and accumulates on the seafloor (e.g., Suess, 1980; Rixen et al., 2019a, b).

55 Upwelling zones affect the marine carbon cycle by sequestering carbon and exchanging carbon between the ocean
56 and the atmosphere via the dissolved inorganic carbon system and $p\text{CO}_2$ changes (Rixen et al., 2006; Krapivin and
57 Varotsos, 2016; Wang et al., 2015). Increased photosynthesis-driven primary productivity during upwelling
58 produces high organic carbon export from the photic zone into the deep sea through the organic carbon pump
59 (Volk and Hoffert, 1985; Ridgwell and Zeebe, 2005). Primary producers account for most of the biomass in
60 upwelling zones, with phytoplankton accounting for > 80% of the particulate organic carbon (Head et al., 1996).
61 Calcification by these primary producers and heterotrophic organisms feeding on them is further an important
62 contributor to the in-organic carbon cycle of the oceans (Falkowski, 1997; Raven and Falkowski, 1999; Ridgwell
63 and Zeebe, 2005; Millero, 2007). However, the productivity of coastal upwelling zones highly depends on
64 atmospheric conditions as they are primarily wind-driven. Consequently, wind-driven upwelling further
65 constitutes a direct intersection between the oceans and the atmosphere. Hence, changes in average wind speeds
66 are directly responsible for the intensity and size of upwelling zones (Dugdale, 1972; Shimmield, 1992; Tudhope
67 et al., 1996; Balun et al., 2010). Therefore, these atmospheric processes may also influence the community
68 structure of primary producers and consumers within the area affected by upwelling.
69 (Lee et al., 1998; Honjo et al., 1999; Munz et al., 2017; Rixen et al., 2019b) today, the Western Arabian Sea (WAS)
70 upwelling is one of the most productive marine regions (Lee et al., 1998; Honjo et al., 1999; Munz et al., 2017;
71 Rixen et al., 2019b). Its high productivity and organic matter flux fuels the Arabian Sea oxygen minimum zone
72 (OMZ), which extends southwards from the Oman Margin between 200 and 1000 m water depth, reaching as far
73 south as 10°N (Morrison et al., 1998; McCreary et al., 2013), making it one of the largest oxygen deficient zones
74 in the modern ocean.

75 Primary productivity in the WAS is furthermore driven by seasonal winds flowing norward along the east coast of
76 Africa (Currie et al., 1973; Rixen et al., 2019a) as an extension of the Somali/Findlater Jets (Sarr et al., 2022;
77 Findlater, 1969). Upwelling in the WAS is thus directly forced by the cross-hemispheric circulation system of the
78 Indian Summer Monsoon (Findlater, 1969; Woodward et al., 1999; Basavani, 2013; Sarr et al., 2022). The
79 prevailing southwesterly winds in the region during the summer months result in the displacement of large water
80 masses (Tudhope et al., 1996; Schott and McCreary, 2001; Schott et al., 2009; Lahiri and Vissa, 2022), resulting
81 in pronounced, intense upwelling peaks during the summer monsoon season (Lee et al., 1998; Honjo et al., 1999;
82 Rixen et al., 2019b). During the northern hemisphere winter, the prevailing wind direction in the Arabian Sea
83 reverses as a weaker and dryer winter monsoon becomes established (Gadgil, 2018). The northeasterly winter
84 monsoon winds result in an additional, albeit less pronounced, productivity spike in the region (Madhupratap et
85 al., 1996; Munz et al., 2015, 2017; Rixen et al., 2019b). Between these two regimes – the inter-monsoon season –
86 weak and variable winds dominate, permitting the establishment of well-stratified regions in the WAS that exhibit
87 oligotrophic surface water conditions. The shift between the different conditions generates a complex pattern of
88 abundance shifts between nutrient-adapted and primarily meso- but potentially even oligotrophic phytoplankton
89 communities. This dynamic impact of changes in wind regimes and upwelling intensity on plankton communities
90 in the WAS is well-established for the modern (Schiebel et al., 2004).

91 In the Arabian Sea, significant variability in productivity has been identified over Pleistocene glacial-interglacials.
92 For example, higher productivity in the Late Pleistocene is associated with interglacial periods (Schubert et al.,
93 1998; Pourmand et al., 2007; Avinash et al., 2015; Naik et al., 2017). Conversely, these climatically driven changes
94 in primary productivity affect the volume of the oxygen minimum zone (OMZ) and the intensity of denitrification
95 in the region (Gaye et al., 2018). An OMZ is the result of the complete consumption of dissolved in the water

96 column due to the microbial degradation of sinking organic matter. Hence OMZ strength is generally related to
97 the strength of primary productivity and, thus, organic matter flux within the overlying upwelling cell (Dickens
98 and Owen, 1994; McCreary et al., 2013; Stramma et al., 2008)

99 Based on current records, the earliest activity within the upwelling zone may have occurred earlier in the
100 Burdigalian (Bialik et al., 2020b). However, it was not until connectivity to the proto-Mediterranean was
101 terminated, and the Arabian Peninsula began to emerge that the regional geographic configuration allowed the
102 establishment of a strong upwelling cell driven by the Findlater Jets (Rögl, 1999; Reuter et al., 2013; Harzhauser
103 et al., 2007; Bialik et al., 2019; Sarr et al., 2022). After the Miocene Climatic Optimum (MCO) ~14 Ma (Flower
104 and Kennett, 1994; Frigola et al., 2018; Sossian and Lear, 2020), global cooling resumed, and a stable, upwelling
105 zone and a sustained OMZ resembling present-day conditions were reported to have established in the WAS
106 (Kroon et al., 1991; Zhuang et al., 2017; Bialik et al., 2020a).

107 Modelling studies suggest that the inception of upwelling and the WAS was closely linked to the tectonic evolution
108 of the Arabian Peninsula, which resulted in water displacement by the Findlater Jet along a newly emergent
109 coastline of Oman (Zhang et al., 2014; Sarr et al., 2022). Therefore, the uplift of the Arabian Peninsula is now seen
110 as the dominant controlling factor for the inception of monsoonal upwelling in the WAS, which is now also **seen**
111 as largely separate from prevailing monsoonal rainfall patterns (Sarr et al., 2022). After the tectonic configuration
112 of the Arabian Peninsula was in place, the cross-hemispheric wind patterns of the South Asian Monsoon were
113 subsequently able to drive upwelling in the WAS in a near modern configuration since the MMCT (Bialik et al.,
114 2020a; Betzler et al., 2016; Gupta et al., 2015).

115 Evidence suggests that strong upwelling in the Arabian Sea first occurred between the Middle and Late Miocene
116 (Kroon et al., 1991; Huang et al., 2007a; Tripathi et al., 2017; Zhuang et al., 2017; Bialik et al., 2020a; Alam et
117 al., 2022). To date, manganese redirection – i.e., the depletion of Mn in the sedimentary record due to Mn-reduction
118 in the water column and subsequent advective transport to the edges of the OMZ – is one of the most used proxies
119 to define OMZs and their past extent within the ocean (Dickens and Owen, 1994). Together with sedimentological
120 facies and micropaleontological studies (Dickens and Owen, 1999; Gupta et al., 2004) these methods have been
121 used effectively to track the size of the OMZ throughout the Indian Ocean and, by proxy, also the intensity of
122 upwelling derived primary productivity. $\delta^{15}\text{N}$ values $> 6 \text{ ‰}$ are seen as possible indicators for significant water
123 column denitrification within the OMZ based on the approach of Tripathi et al. (2017). Bialik et al. (2020a) applied
124 this approach **for** a Middle to Late Miocene interval at Site 722, showing that upwelling in the WAS may have
125 sustained an OMZ strong enough for denitrification to occur as early as 11 Ma ago. However, these methods do
126 not provide direct evidence **for** how changing wind and nutrient levels have interacted to result in the observed
127 OMZ pattern.

128 Following these lines of evidence, it can be summarized that WAS upwelling initiated during the Middle to Late
129 Miocene during the **Middle Miocene Climatic Transition (MMCT)**, marked by cooling sea surface temperatures
130 (SSTs) since ~14.7 Ma (Zhuang et al., 2017; Holbourn et al., 2014, 2015). Monsoonal winds subsequently
131 intensified only after the MMCT at ~13 Ma, in conjunction with OMZ expansion to the Maldives (Betzler et al.,
132 2016) before reaching maximum intensity at ~11 Ma and potentially declining at ~9 Ma (Bialik et al., 2020a).
133 Upwelling re-intensified later in the Miocene and oscillated into the Plio-Pleistocene (Kroon et al., 1991; Huang
134 et al., 2007b; Gupta et al., 2015; Tripathi et al., 2017; Alam et al., 2022). The Serravallian upwelling intensification
135 is accompanied by significantly increased biogenic silica accumulation across the northern Indian Ocean (Keller
136 and Barron, 1983; Baldauf et al., 1992). This biogenic silica bloom is dominated by siliceous plankton such as

137 diatoms and radiolaria (Nigrini, 1991), indicating a sustained regime of high nutrient levels, which was able to
138 support these primary producers (Blain et al., 1997; Schiebel et al., 2004; Mikaelyan et al., 2015).
139 The present study aims to better constrain the relationships and interactions between different plankton groups in
140 the WAS within the context of the dynamic changes occurring in the Oman Margin upwelling cell throughout the
141 Middle to Late Miocene.

142 2. ODP Site 722 – Site location, age model, and oceanographic setting

143 Ocean Drilling Project (ODP) Site 722 (16°37'18.7" N/59°47'45.33" E) lies offshore Oman on the Owen Ridge, a
144 300-km-long and 50-km wide feature in the WAS (Fig. 1a). Site 722 is located at a water depth of 2027.8 m
145 (Shipboard-Scientific-Party, 1989) at the edge of the present-day Oman upwelling zone (Fig. 1a), and lies below
146 the core of the Indian Ocean Oxygen Minimum Zone (OMZ), with oxygen concentrations $< 2 \mu\text{mol kg}^{-1}$ persisting
147 at a depth between c. 200 – 1000 m water depth (McCreary et al., 2013; Garcia et al., 2018).

148 The sedimentary cover at the site location comprises nanofossil, foraminifer, and diatom-rich pelagic oozes, with
149 silty clay (Shipboard-Scientific-Party, 1989; Rodriguez et al., 2014; Bialik et al., 2020a). Bialik et al. (2020a)
150 recently published a revised age model for Site 722, which we will utilize throughout this study. The age-depth
151 correlation relies on biostratigraphic information from the nanofossil assemblage data used in this study,
152 combined with existing shipboard data (Shipboard-Scientific-Party, 1989). The age model covers the study interval
153 over the Middle Miocene to the Late Miocene (c. 15.0 – 8.5 Ma, corresponding to a core depth of 276.62 to 404.94
154 mbsf). Bialik et al. (2020a) published benchtop x-ray fluorescence (XRF)-based elemental data, total organic
155 carbon content (TOC), and the calcite equivalent carbonate content in the analyzed samples. These geochemical
156 proxy data were subsequently used in conjunction with the nanofossil assemblage data to fully constrain the
157 response of the assemblage to changing environmental conditions in the WAS upwelling zone.

158 The modern-day water mass configuration of the WAS (Fig. 1b) indicates that Indian Central Water (ICW) upwells
159 in the upwelling region offshore **oman**. The ICW result from a mixture of warm, highly saline Red Sea and Persian
160 Gulf Waters (RSPGW), as well as Sub-Antarctic Mode and Intermediate Waters (SAWM, and AAIW
161 respectively). Modern oceanographic research suggests that AAIW/SAMW, which contributes to the ICW is the
162 dominant source of nutrients in the Arabian Sea upwelling region today (Böning and Bard, 2009; Toggweiler et
163 al., 2019a; You and Tomczak, 1993; You, 1997, 1998). In addition, at present, there also exists some contribution
164 of the Indonesian Intermediate Waters (IIW), the ICW in the WAS (Fig. 1a and 1b). Therefore, changes in the
165 supply of these water masses are a critical aspect of understanding the region's past and likely future upwelling
166 dynamics (Böning and Bard, 2009; Laufkötter and Gruber, 2018; Toggweiler et al., 2019b). The Middle to Late
167 Miocene was similar to the modern (Bialik et al., 2019; Hall, 2012). However, the Indonesian Throughflow
168 region's configuration remains largely enigmatic, with potentially large emergent island chains and extensive coral
169 reefs between Australia and South East Asia (Hall, 2012). Deep and Intermediate water exchange and, thus, IIW
170 formation may thus have been restricted in the Miocene. If present, IIW likely would supply additional nutrients,
171 including a significant amount of bioavailable silica, to the upwelling zone in the WAS (You and Tomczak, 1993;
172 You, 1997). Waters in the WAS therefore **represent** mixture of SAMW/AAIW and IIW with ICW, which later
173 intermix with the regionally formed RSPGW (Böning and Bard, 2009; Toggweiler et al., 2019a).

174 3. Methods

175 3.1. Nannofossil and siliceous fragment quantification

176 We produced smear slides from 71 freeze-dried samples taken from Hole 722B (supplemental data 1) following
177 the quantitative drop technique of Bordiga et al. (2015). On each slide, at least 47 field views were counted until
178 at least 300 specimens were recorded or until over 190 field views were reached for samples containing very low
179 abundances. During counting, nannofossils were identified down to the species level whenever possible. The
180 occurrence of diatom frustules (including pennate and centric forms), as well as other biogenic silica fragments
181 (including silicoflagellates and radiolarian fragments), were quantitatively recorded without further taxonomic
182 identification (supplementary data 1). All recorded nannofossil taxa (+ siliceous fragments) were then converted
183 into absolute abundances per g/sediment, according to Bordiga et al. (2015), with portions of the dataset already
184 published (Bialik et al., 2020a). In addition to the above-described quantification, the high amount of biogenic
185 silica recorded in some sections often dilutes absolute nannofossil abundances, to alleviate the issues with potential
186 dilution of nannofossil abundance due to high fluxes of biogenic silica, we calculated nannofossil and siliceous
187 fragment fluxes for the studied interval (see section 3.5).

188 Taxonomic Remarks

189^{3.1.1.} We relied on the Nannotax3 website (Nannotax 3, 2023) for detailed taxonomic reference and identification. In
190 addition, taxonomic identification followed the concepts outlined in Perch-Nielsen (1985) and Young (1998), the
191 Handbook of Calcareous Nannoplankton 1–5 (Aubry, 1984, 1988, 1989, 1990, 1999), and the compilation on the
192 taxonomy of the order Discoasterales by Aubry (2021).

193 For subsequent ecological interpretations, we combined the identified *Reticulofenestra* morphotypes into three
194 size bins ranging from small (<3 µm) to medium (<3-5 µm) and large (>5 µm). There is some debate regarding
195 the taxonomic distinction of the reticulofenestrids (genus *Reticulofenestra*) in the Neogene (see Young, 1998, for
196 discussion). Several research groups (Auer et al., 2019; Gibbs et al., 2005; Imai et al., 2017; Jatingrum and Sato,
197 2017; Wade and Bown, 2006) apply different size ranges to differentiate *Reticulofenestra* taxa based on placolith
198 size. We also note that each of these size ranges may contain a multitude of genotypes (Young, 1998). In this
199 study, we follow the species concept of Auer et al. (2019) adapted for the Middle to Late Miocene:

- 200 • *Reticulofenestra* spp. (small) cf. *R. minuta*: reticulofenestrids < 3 µm in length without a bar spanning the
201 central area.
- 202 • *Reticulofenestra haqii*: reticulofenestrids 3–5 µm in length with an open central area.
- 203 • *Reticulofenestra antarctica*: reticulofenestrids 3–5 µm in length with a closed central area.
- 204 • *Reticulofenestra pseudoumbilicus* (small): all reticulofenestrids 5–7 µm in length.
- 205 • *Reticulofenestra pseudoumbilicus* (sensu stricto): all reticulofenestrids >7 µm in length.

206 3.2. Planktonic foraminifera counts and quantification

207 For foraminifera analysis, 28 samples were freeze-dried, weighed, and wet-sieved using mesh sizes 250, 125, and
208 63 µm. After sieving, sample residues were oven dried at 40°C. For quantitative foraminiferal analyses, the size
209 fractions > 250 µm and 250-125 µm were examined under a stereomicroscope (Zeiss V8). In each sample, at least
210 200 specimens were picked and identified. In 8 samples, less than 200 specimens were found in the available
211 material. When necessary, samples were split into smaller aliquots (splits). The total number of foraminifera in the

212 sediment (N/g) was calculated from the number of the counted specimen and the number of splits. Relative
213 abundances (%) were calculated for each species (see supplementary data 2 for details).

214 **3.3. Statistical Analyses and Ordination**

215 All applied statistical and ordination methods were performed using PAST4 (v. 4.11 released 2022-09-13; Hammer
216 et al., 2001). The applied methods include correlation matrices between nannofossil taxa and XRF-based
217 environmental proxy data for dust flux and Mn depletion, the abundance of siliceous fragments, and calcite
218 equivalent CaCO_3 content (supplementary data 3). Percentage data were then arcsine-transformed before cluster
219 analyses and ordination methods. The arcsine transformation was applied to generate a statistically viable dataset
220 suitable for the applied clustering and ordination methods (Sokal and Rohlf, 1995; Hammer and Harper, 2006;
221 Auer et al., 2014, 2019; Bialik et al., 2021) and applies the universal paired group method with arithmetic mean
222 (UPGMA) with Bray-Curtis distance. Cluster stability was further evaluated by using UPGMA clustering with
223 Euclidian distance and Ward's method.

224 The contributing taxa of each cluster were subsequently evaluated based on similarity percentage (SIMPER)
225 analysis (Bray-Curtis similarity). The correspondence of nannofossil variability within each sample with
226 environmental parameters was investigated using the non-metric multidimensional scaling (nMDS), where
227 geochemical proxy data (see sect. 2; Fig. 3) were used as environmental variables and visualized as vectors within
228 the two-dimensional coordinate space of the nMDS. Additionally, several diversity indices (see supplementary
229 data 1), including the Shannon H' -diversity, were automatically calculated for the calcareous nannofossil
230 assemblage (Hammer and Harper, 2006).

231 **3.4. Published geochemical proxy data used in this study**

232 In addition to the paleobiological data generated for this study, we further apply a suite of previously published
233 geochemical proxy data (Bialik et al., 2020a), which we utilize as additional lines of evidence to anchor the
234 observed assemblage variation within a multiproxy framework. In brief, we apply CaCO_3 and TOC combined
235 with fluxes of siliceous fragments (see section 3.5 for details), as productivity proxies. Benchtop x-ray
236 fluorescence-derived elemental ratios further supplement this interpretation, where we apply Mn/Al ratios to
237 quantify Mn redirection (see Bialik et al., 2020a), based on the model of Dickens and Owen (1994). The available
238 XRF data was also used to generate a dust flux proxy based on the elemental ratio of $(\text{K}+\text{Al})/(\text{Fe}+\text{Ti}+\text{Zr})$, as
239 defined by Kuhnt et al. (2015). This dust flux proxy allows determining the accumulation of Fe, Ti and Zr bearing
240 heavy mineral phases, compared to elements predominantly present in clay minerals (Al + K). We interpret this
241 proxy as a qualitative proxy for wind-derived dust flux and, thus, varying wind strength at Site 722. Dustflux and
242 wind speed are intrinsically linked to Africa's progressive aridification due to the uplift of the Arabian Peninsula
243 (Zhang et al., 2014; Sarr et al., 2022). The published $\delta^{15}\text{N}$ is also discussed in the context of the new assemblage
244 data. Tripathi et al. (2017) interpret $\delta^{15}\text{N}$ values $> 6 \text{ ‰}$ as an indicator for significant water column denitrification
245 in ocean basins with oxygenated bottom waters. Later, Bialik et al. (2020a) also used this proxy interpretation for
246 the Middle to Late Miocene interval at Site 722, which will be followed herein.

247 3.5. Calculation of accumulation rates and fluxes

248 To quantify flux rates we applied moisture and density (MAD) derived bulk density data generated during Leg
249 117 (Shipboard-Scientific-Party, 1989), to calculate mass accumulation rates (MAR). To calculate bulk MARs we
250 applied linear interpolated dry bulk density for each sample point using the calculation

$$251 \quad BMAR = \frac{DBD \times LSR}{10}$$

252 Where BMAR is the bulk mass accumulation rate in g/cm²/kyr, and DBD is the dry bulk density in g/cm³ based
253 on shipboard MAD data, and LSR is the linear sedimentation rate in m/myr calculated based on the age model of
254 Bialik et al. (2020a). Thusly generated bulk MARs were subsequently used to also calculate mass fluxes of TOC,
255 CaCO₃ given as g/cm²/Ma. Fossil fluxes are given as nannofossil accumulation rates (NAR) as well as diatom
256 accumulation rates (DAR), which are calculated by multiplying the BMAR with the number of individuals per g
257 of sediment.

258 4. Results

259 4.1. Calcareous Nannofossils

260 Nannofossil abundance, diversity

261^{4.1.1.} Nannofossil preservation found to be good to moderately good based on visual evaluation using light and scanning
262 electron microscopy. Overall preservation in biogenic-silica-rich samples was noted to be slightly poorer than in
263 samples with little or no biogenic silica.

264 Total nannofossil fluxes range from 4.77*10⁸ to 9.93*10¹⁰ liths/cm²/Ma, with an average of 1.45*10¹⁰ and a median
265 of 1.07*10¹⁰. By comparison, total nannofossils per g/sed. range from 2.75*10⁸ to 4.11*10¹⁰ with an average of
266 5.73*10⁹ and a median of 4.04*10⁹. Diatom accumulation range from no frustules to 2.41*10¹⁰ frustules/cm²/kyr,
267 with an average of 2.24*10⁹ and a median of 3.72*10⁸. In the three uppermost samples taken from Core 722B-
268 30X, small placolith abundance (primarily *Reticulofenestra minuta*) increases sharply above the base absence (Ba)
269 of *Reticulofenestra pseudoumbilicus* (Backman et al., 2012; Agnini et al., 2017) after 8.8 Ma (Fig. 2). For details
270^{4.1.2.} on the abundance and variability of individual nannofossil taxa, please refer to the supplementary material
271 (supplementary data 1).

272 Clusters and Ordination

273 Cluster analysis (UPGMA, Bray-Curtis similarity) resulted in 4 major clusters (clusters 1-4) that were defined at
274 a similarity cutoff of 0.61 with a cophenetic correlation coefficient of 0.81. Clusters 1 and 4 were again split into
275 2 (clusters 1a-b) and 3 (clusters 4a-c) sub-clusters, respectively, at a similarity cutoff of 0.66 (Fig. 4a).
276 Bootstrapping (N=1000) shows weak support for individual clusters reflecting the overall strong similarities in the
277 assemblage composition of the studied samples. However, one-way ANOSIM shows p-values of <0.05, indicating
278 that the separated clusters are statistically significant.

279 Based on SIMPER analysis, the clusters and subclusters are primarily defined by the abundance variability of
280 reticulofenestrids, discoasterids, *Cyclicargolithus floridanus*, and, to a smaller extent, *Coccolithus pelagicus*, and
281 *Sphenolithus* spp. Based on these results, we infer that the clusters represent taphogroups, each reflecting different
282 environmental conditions (see Auer et al., 2014).

283 Taphogroup (TG) 1a is characterized by a very high abundance of small reticulofenestrads. TG 1b is similarly
284 characterized by a high abundance of small reticulofenestrads, although lower than TG 1a, with a higher abundance
285 of medium reticulofenestrads and *Cyclicargolithus floridanus*. TG 2 is characterized by a high abundance of *C.*
286 *floridanus*, and TG 3 by a high abundance of large reticulofenestrads with common discoasterids. TG 4 and its
287 subgroups are primarily defined by the variation of the three size ranges of reticulofenestrads, with TG4a exhibiting
288 the highest abundances of small reticulofenestrads, TG4b showing the lowest amounts of both small and medium
289 reticulofenestrads, and through TG4c high numbers of both medium and large reticulofenestrads. See table 1 for a
290 summary of the TGs and the supplementary material (supplementary data4) for a statistical breakdown of the
291 contribution of all taxonomic groups to each TG.

292 The cluster analysis results are well represented within the nMDS, with TGs splitting well along coordinates 1 and
293 2. Furthermore, the recorded stress of the nMDS is 0.13, indicating that the results are robust (Clarke, 1993). We,
294 however, note the overall high compositional similarity of clusters, particularly sub-clusters, which results in
295 higher stress in the nMDS. This is important, as recently a more conservative approach has been put forward,
296 recommending that nMDS outputs exhibiting stress above 0.1 should be carefully evaluated (Bialik et al., 2021).
297 We found a positive loading for TOC, and siliceous fragments, along coordinates one and two. Dustflux, calculated
298 as $\ln((Zr+Ti+Fe)/(Al+K))$ following Kunt et al. (2015), is positively loaded on coordinate one but negatively
299 loaded on coordinate two. The Mn/Al ratio is loaded negatively on coordinate 1 and positively on coordinate 2.
300 Whereas CaCO₃ is loaded negatively on both coordinates (Fig. 4b).

301 4.2. Planktonic Foraminifera

302 Out of 28 samples one sample (722B-34X-3W 30-32, ca. 10.2 Ma) was barren in planktonic foraminifera. In the
303 remaining 27 samples, 27 taxa of planktonic foraminifera were identified. The planktonic foraminifera
304 preservation was overall good, but decreases downhole. The foraminifera tests were found to be moderately
305 pyritized. Of these taxa, 5 (*Globigerinoides ruber*, *Globorotalia menardii*, *Neogloboquadrina acostaensis*,
306 *Paragloborotalia mayeri*) have their stratigraphic first or last occurrence within the studied interval. All recorded
307 taxa were grouped according to their environmental preferences following established environmental assignments
308 of either mixed layer taxa, open ocean thermocline taxa, open ocean sub-thermocline taxa, upwelling taxa, or
309 unknown (Table 2).

310 Through the studied interval, thermocline species and mixed layer taxa are the most abundant (abundance reaches
311 more than 50%). Both mixed layer and upwelling taxa increase in prevalence through the studied interval, while
312 thermocline species decrease. A sharp drop in thermocline taxa occurs between 11 Ma and 10 Ma, corresponding
313 to the disappearance of *Paragloborotalia mayeri*, the dominant taxa until that time. Mixed layer taxa remain at a
314 near-stable level from 11 Ma onwards. Upwelling taxa are not represented in two samples between 11 Ma and
315 10.8 Ma, after which this group exhibits a steady increase until the end of the studied interval. Sub-thermocline
316 taxa are present between 9.0 Ma and 9.5 Ma and account for only a small fraction (less than 3% at most)
317 of the assemblage.

318 **5. Discussion**

319 **5.1. Definition of taphogroups and their paleoenvironmental significance**

320 Based on the above results, we interpret the analyzed samples in the context of their taphogroups. Taphogroups
321 represent the total preserved fossil assemblage deposited at a given time in the past. Samples assigned to contain
322 the same taphogroup can therefore be assumed to reflect similar local surface water conditions at Site 722.

323 **Taphogroup 1a:** TG1a is dominated by small reticulofenestrads. We, therefore, interpreted this TG as
324 indicative of high nutrient levels facilitating the proliferation of small bloom-forming placoliths (primarily
325 *Reticulofenestra minuta*; see Table 1). Small reticulofenestrads are commonly associated with high
326 terrigenous nutrients in near-shore environments (see references in Table 1). However, as Site 722 was
327 always located in the open ocean and sedimentological data (Bialik et al., 2020a) does preclude a change
328 in terrigenous nutrient sources, a different mechanism must be invoked for this dominance of small
329 reticulofenestrads. Studies based on coccolithophore cultures indicate that the proliferation of small
330 placoliths may result from nitrogen limitation in a highly productive open marine environment. For
331 example, Paasche (1998) showed that modern-day coccolithophores tend to increase the formation of small
332 placoliths during N-limitation. Hence, we assume that the proliferation of small reticulofenestrads in the
333 open ocean results from increasing nitrogen limitation compared to other macro- or micronutrients. Such
334 N-limited environments often persist in settings with high productivity, due to rapid N-loss during
335 denitrification (Paerl, 2018), which would fit with the above interpretation of small Reticulofenestrad
336 proliferation at Site 722, offshore Oman.

337 **Taphogroup 1b:** The presence of common *C. floridanus* in combination with abundant small and medium-
338 sized reticulofenestrads within this assemblage indicates elevated nutrient levels, compared to a fully
339 oligotrophic assemblage (see Table 1). The very high but not dominant abundance of small
340 reticulofenestrads may also point to N-limited nutrient sources (see TG 1a). This will be analogous to the
341 fringes of the modern-day Arabian Sea upwelling cell, where nitrogen may be the primary limiting nutrient
342 (Anju et al., 2020), hinting at the presence of more **coastally** confined upwelling during TG1b, which did
343 not fully reach Site 722. The overall high diversity, compared to other TGs, suggests that **also oligotrophic**
344 conditions may have ~~persisted~~ at times (likely **seasonally**), which may also point towards phosphate co-
345 **limitation** at times where upwelling was limited. We thus interpret TG 1b as reflective of open marine
346 conditions with only somewhat elevated nutrient levels compared to an open ocean gyre. Primary nutrient
347 supply, however, is still controlled by nutrients derived through the remineralization of locally produced
348 particulate organic matter (Cullen, 1991), likely supplied to the surface water through seasonal mixing
349 during limited summer monsoons.

350 **Taphogroup 2:** Within TG 2, common *C. floridanus* occurs together with medium and large
351 reticulofenestrads, commonly associated with warmer water temperature, a deep nutricline, and potentially
352 elevated nutrient conditions. Therefore, we interpret this TG to reflect open marine conditions without
353 directly indicating upwelling-derived nutrients. Nutrients were likely mainly derived through POM
354 remineralization, with low external nutrient influx through upwelling or terrigenous nutrients.

355 **Taphogroup 3:** Previous studies (Auer et al., 2014; Lohmann and Carlson, 1981) generally associated large
356 reticulofenestrads with high nutrient conditions. Imai (2015) states that dominant large reticulofenestrads

357 and common discoasterids indicate low nutrient conditions and a deep nutricline compared to a high
358 abundance of small reticulofenestrads.
359 However, this interpretation is questioned by the association of TG 3 with high TOC, high dust flux, and
360 high silica accumulation rates, indicating strong upwelling conditions (Fig. 4b). Although, similar co-
361 occurrences of diatoms and discoasterids were previously recorded in the eastern equatorial pacific and the
362 Mediterranean (Backman et al., 2013).
363 While difficult to ascertain, the association of TG 3 with high dust flux and thus additional iron fertilization
364 may represent exceptionally high primary productivity (Guieu et al., 2019). Furthermore, modern analogs
365 based on large *Geophyrocapsa* taxa, descendants of the genus *Reticulofenestra* (Samtleben, 1980; Perch-
366 Nielsen, 1985; Nannotax 3, 2023), are more abundant in high nutrient upwelling zones (Bollmann, 1997).
367 Seasonality, between summer monsoon and weak or absent winter monsoon however, could also serve to
368 partially address this discrepancy in the interpretation of TG 3 with available environmental data. Diatom
369 and coccolithophore accumulation occur in such a setting in different nutrient regimes. Modern-day culture
370 studies of coccolithophores (Paasche, 1998) also show that the calcification of coccolithophores increases
371 during nitrogen excess and phosphate limitation.
372 Therefore, we interpret TG 3 as indicative of likely the strongest summer monsoon controlled upwelling
373 for our Middle to Late Miocene study interval. Conversely, a still relatively weak winter monsoon resulted
374 in a deep nutricline during the rest of the year.
375 **Taphogroup 4a:** Taphogroup 4a is not dominated by a specific reticulofenestrad size range while also
376 containing a diverse assemblage in general (see Table 1). We, therefore, interpret this TG to show weaker
377 upwelling conditions compared to TG3 or TG 1a during transient climatic conditions. Furthermore, weaker
378 productivity is implied by a stronger association of TG 4a with higher Mn/Al values (Fig. 4b).
379 **Taphogroup 4b:** The high dominance of large reticulofenestrads of TG 4b would suggest elevated,
380 upwelling-derived nutrient levels in a temperate upwelling zone (see TG3 above). Furthermore, the size of
381 experimental studies of calcification rates by Paasche (1998) may also be indicative of p-limitation. High
382 nutrient conditions are corroborated by the general association of TG 4b with siliceous fragments, TOC,
383 and dust flux in the nMDS (Fig. 4b).
384 **Taphogroup 4c:** Taphogroup 4c is defined by both medium and large reticulofenestrads (Table 1,
385 supplementary material). Therefore, we interpret this TG as indicative of weaker but sustained upwelling
386 conditions. In addition, it shows some association with upwelling indicators such as dust flux and no
387 association with the Mn/Al ratio in the sediment (Fig. 4b), indicating that it only is associated with a overall
388 active upwelling zone and and active Mn-ridirect and therefor OMZ conditions at Site 722.

389 5.2. Temporal Progression of Environmental Changes

390 Individual taphogroups represent specific ecospace, but to understand the relation and transitions between these
391 ecospace, in their temporal context, their variability has to be considered in relationship to other proxies within a
392 multi-proxy approach. Integrating the analyses of nannofossil taphogroups (Table 1), planktonic foraminifera data
393 (Fig. 5), the abundance of diatom fluxes and geochemical data (Bialik et al., 2020a), we delineate temporal
394 intervals in Site 722. These reflect stratigraphic intervals of specific environmental conditions in the WAS.

395 **Interval 1 (Base of study interval – 13.4 Ma):** This interval is characterized by variable taphogroups belonging to
396 TG 1a, TG 2, TG 4a, and TG 4b. The variable taphogroups reflect a diverse and variable nannofloral assemblage

397 in this interval. Overall the nannofloral assemblages are characterized by an high abundance of *Cyclicargolithus*
398 *floridanus* (Fig. 5). However, *Cyclicargolithus floridanus* abundances decline through the interval to its
399 stratigraphic Top (T) occurrence at Site 722. In addition, we record abundant small reticulofenestrids and peaks of
400 discoasterids (TG 4a, 4b). The average number of taxa in interval 1 is 14.9 ± 2.1 ($N = 13$), with an average Shannon
401 H' diversity of 1.6 ± 0.4 . The planktonic foraminifera assemblage is dominated by thermocline-dwelling taxa
402 (predominantly *P. mayeri*). Siliceous fragments are absent. We interpret this interval as a relatively low nutrient
403 environment based on the above multi-group assemblage composition. In particular, the presence of TG 1a and 2
404 points to only moderately elevated nutrient concentrations in the surface waters at Site 722 during MMCT. The
405 common occurrence of *Sphenolithus* spp. and discoasterids suggests intermitted – potentially seasonal –
406 stratification. These results are consistent with the relatively warm SSTs recorded during this interval (Zhuang et
407 al., 2017), further supporting a generally muted upwelling regime in the WAS during interval 1. These assumptions
408 are corroborated by a more limited OMZ extent in the Indian Ocean, compared to the later Miocene. At Site 722
409 this is shown declining Mn content. On the Maldives, high Mn concentrations as well as the absence of notable
410 drift deposits, and thus lower wind intensity, also corroborates a generally weaker OMZ during this time (Bialik
411 et al., 2020b; Betzler et al., 2016).

412 **Interval 2a (13.4 – 12.0 Ma):** Interval 2a is solely comprised by TG 4c. This taphogroup is characterized by a
413 diverse assemblage with abundant *R. pseudoumbilicus* and common medium-sized reticulofenestrids and
414 discoasterids. The average number of taxa is 16.6 ± 2.2 ($N = 7$), with an average Shannon H' index of 1.8 ± 0.3 .
415 Siliceous fragments are absent.

416 Planktonic foraminiferal assemblages are dominated by thermocline species with increased abundances of mixed
417 layer species compared to interval 1. Within interval 2a, a first slight increase in upwelling indicative taxa
418 (primarily *G. bulloides*) is observed. We interpret this interval as indicative of a first shallowing of the thermocline
419 due to the initial strengthening of the wind-driven upwelling regime at Site 722. This intensification is likely related
420 to an intensification of the monsoon system following the end of the MMCT (Betzler et al., 2018). The
421 intensification of the monsoon system is also consistent with the establishment of an increased OMZ extent and
422 drift deposits in the Maldives (Betzler et al., 2016).

423 **Interval 2b (12.0 Ma – 11.0 Ma):** Interval 2b comprised primarily of assemblages belonging to TG 4c, with one
424 sample belonging to cluster 1b. The interval similar to interval 2a is characterized by assemblages (TG4c) with
425 abundant medium-sized reticulofenestrids that occur together with an increase in large reticulofenestrids.
426 Furthermore, we detect a low but noteworthy increase in *Umbilicosphera jafari* and a decline in Discoasteraceae.
427 Furthermore, the abundance of small reticulofenestrids is lower than in interval 2a. These differences within the
428 assemblage are also the reason why interval 2 was separated into the two sub-intervals. The average number of
429 taxa in interval 2b is 15.6 ± 2.6 ($N = 16$), with an average Shannon H' index of 1.5 ± 0.3 . The base of interval 2b
430 also contains the first occurrence of diatoms within the section. Planktonic foraminifera mixed layer taxa decrease
431 noticeably while upwelling taxa further increase in this interval.

432 We interpret this interval to mark a progressive intensification in the upwelling of high-nutrient subsurface waters.
433 We base this on 1) the increase in siliceous fragments (diatoms and other siliceous biota, 2) higher abundances of
434 upwelling indicative planktonic foraminiferal taxa, 3) generally nutrient-adapted nannofossil taxa (i.e., medium
435 and large sized reticulofenestrids; Beltran et al., 2014; Auer et al., 2015; Imai et al., 2015) show progressive
436 abundance increases. Intensified upwelling is consistent with increasing $\delta^{15}\text{N}$ values and continuous cooling at
437 Site 722 (Zhuang et al., 2017; Bialik et al., 2020a). Increased upwelling-derived nutrient access in the northern

438 Indian Ocean is further supported by increased productivity and nitrogen utilization in the Maldives (Betzler et al.,
439 2016; Ling et al., 2021). The upwelling intensification after 12 Ma is consistent with an overall increase in global
440 atmospheric circulation and oceanic current strength, including the Indian Ocean south equatorial current (Fig. 6;
441 House et al., 1991; Gourelan et al., 2008; Groeneveld et al., 2017; Betzler and Eberli, 2019).

442 **Interval 3a (11.0 Ma – 9.6 Ma):** Interval 3a is characterized by a dominance of large reticulofenestrads (*R.*
443 *pseudoumbilicus*) (TG 3) with intermittently common discoasterids and small reticulofenestrads (TG 4b). Notably,
444 medium-sized reticulofenestrads show very low abundances compared to the previous intervals. The abundance of
445 *Umbilicosphaera jafari* is highly variable but overall common, while sphenoliths are rare in the lower part of the
446 interval before increasing (up to ~ 40 % of the assemblage) in the upper part. Within this interval, we also note the
447 occurrence of variable abundances of small reticulofenestrads between ~10.5 to 9.9 Ma. The average number of
448 taxa is 14.3 ± 5.1 ($N = 22$), with an average Shannon H' index of 1.1 ± 0.4 . The high environmental variability
449 within this interval is illustrated by alternations between assemblages belonging to TG 3, 4b, and 4c. Diatom fluxes
450 increase significantly (Fig. 5). Diatoms generally dominate the phytoplankton assemblage, even outcompeting
451 calcareous nannoplankton in terms of total abundance. High diatom abundances are especially prevalent within
452 samples assigned to TG 3. Mixed layer taxa dominate planktonic foraminifera assemblages and increase in this
453 interval, together with upwelling taxa. Notably, thermocline species decline to less than half of their previous
454 abundance. One sample (722B-34X-3W 30-32) is barren of planktonic foraminifera. The lack of foraminifera is
455 likely due to the limited sample amounts washed for this study, in conjunction with the high accumulation rates of
456 phytoplankton (diatoms and calcareous nannofossils) in this stratigraphic interval.

457 Based on the high abundance of diatoms and a generally high nutrient-adapted nannofossil assemblage, we
458 interpret interval 3a as a peak in upwelling intensity at Site 722. This interpretation is consistent with previously
459 published $\delta^{15}\text{N}$ data from Site 722 and Sites U1466 and U1468, and other geochemical datasets in the Maldives
460 (Bialik et al., 2020a; Ling et al., 2021). In addition, high productivity and OMZ expansion are further recorded by
461 heightened TOC, Uranium accumulation, and low Mn deposition within the northwestern Indian Ocean (Dickens
462 and Owen, 1994, 1999; Betzler et al., 2016; Bialik et al., 2020a). This corresponds to an increase in Antarctic
463 Bottom Water (AABW) formation due to the expansion of North Atlantic Deep Water (NADW), indicative of an
464 intensified global thermohaline circulation (Woodruff and Savin, 1989). Increasing numbers of discoasterids in
465 the upper part of interval 3a, and decreasing diatoms numbers also point towards declining upwelling and, thus,
466 seasonal nutrient depletion when no summer monsoon-derived upwelling occurs. This pattern of clear seasonality
467 imparted on the plankton flux further amplifies within the next interval.

468 **Interval 3b (9.6 Ma – 8.8 Ma):** Interval 3b continues to exhibit a dominance of large reticulofenestrads (*R.*
469 *pseudoumbilicus*) (TG 3), although discoasterids noticeably decline and are replaced by higher abundances of
470 sphenoliths (primarily *Sphenolithus moriformis*), with abundances of ~ 40 % of the total assemblage. Small- and
471 medium-sized reticulofenestrads are rare in this interval. The average number of taxa is 15 ± 2.3 ($N = 10$), with an
472 average Shannon H' index of 1.4 ± 0.3 .

473 We thus interpret interval 3b to indicate decreasing upwelling intensity based on the increase in nannofossil taxa
474 adapted to warmer and more stratified water masses, such as *Discoaster* spp. and *Sphenolithus* spp. (Lohmann and
475 Carlson, 1981; Castradori, 1998; Negri and Villa, 2000; Blanc-Valleron et al., 2002; Gibbs et al., 2004a; Aubry,
476 2007; Villa et al., 2008; Schueth and Bralower, 2015). The waning upwelling of the northern Indian Ocean is
477 corroborated by the proliferation of warm water diatom taxa in the Maldives (Site 714; Boersma and Mikkelsen,
478 1990). Decreasing $\delta^{15}\text{N}$ values support waning upwelling-derived productivity after 10 Ma at both Site 722 and in

479 the Maldives and decreasing TOC fluxes at Site 722 (Gupta et al., 2015; Bialik et al., 2020a; Ling et al., 2021). It
480 is, however, important to note that these changes are not reflected in the planktonic foraminifera community, which
481 shows a continuously high presence of upwelling taxa (e.g., *G. bulloides*). One possibility would be that the
482 upwelling cell became more seasonal, with nanoplankton-dominated photoautotrophic communities proliferating
483 seasons with lower upwelling. However, primarily heterotrophic, non-symbiont-bearing taxa such as *G. bulloides*
484 were still sustained by high primary productivity during monsoon season, as is the case in the present-day
485 upwelling cell along the Oman Margin (Schiebel et al., 2004; Rixen et al., 2019b).

486 We assume that this waning in upwelling is related to a decrease in the hemispheric temperature gradients leading
487 to a weaker summer monsoon wind system in the Indian Ocean. This reduction in temperature gradients is
488 consistent with a decreasing trend in minimum deep-water temperatures, based on global benthic foraminifera
489 compilations and deep-water records from the ninety-east-ridge (Site U1443; Fig. 1) (Lübbers et al., 2019;
490 Westerhold et al., 2020). Furthermore, pollen data (Pound et al., 2012) suggests that progressive cooling of the
491 northern hemisphere (NH) over the Middle to Late Miocene intensified. Northern hemisphere cooling
492 consequently reduced the asymmetry of hemispheric temperature gradients, thereby reducing summer monsoon
493 wind intensity by muted northward migration of the intertropical convergence zone (ITCZ) in NH summer (Gadgil,
494 2018; Yao et al., 2023).

495 **Interval 4 (8.8 Ma – top of study interval):** Interval 4 – consisting of only three samples – is defined by the
496 bloom of small reticulofenestrids (*R. minuta*) in the nanofossil assemblage. We also note an elevated abundance
497 of *Umbilicosphaera jafari* and a marked decline in *Sphenolithus* spp. relative to interval 3b. This interval consists
498 entirely of assemblages belonging to TG 1b. The average number of taxa is 17.3 ± 0.5 ($N = 3$), with an average
499 Shannon H' index of 0.5 ± 0.0 . Despite the high number of nanofossil taxa in this interval, the low diversity
500 directly results from the dominance of small reticulofenestrids. Siliceous fragments (primarily diatoms) persist but
501 are much rarer than in interval 3. This reduction in diatom fluxes is part of an ongoing decrease in biogenic silica
502 accumulation at Site 722, which culminates in a shift from phytoplankton to zooplankton-dominated silica
503 accumulation by ~8 Ma (Nigrini, 1991; Prell et al., 1992). Planktonic foraminifera assemblages remain consistent
504 with the upper part of interval 3, showing relatively high abundances of upwelling and mixed-layer taxa. We
505 interpret this interval as a new nutrient regime which likely led to a significant turnover in coccolithophore species
506 around the same time (Young, 1990; Imai et al., 2015). However, the low sample number in this interval limits
507 further interpretation.

508 **5.3. Plankton community responses paleoenvironmental changes**

509 Based on the intervals defined by the nanofossil taphogroups, a progression of plankton communities becomes
510 apparent within the Middle to Late Miocene at Site 722. Their variation highlights the strong interactions between
511 monsoon wind strength, nutrient availability, and primary productivity. Therefore, we link our new assemblage
512 data with an extensive data compilation highlighting a progressive upwelling increase, which leads to thermocline
513 shoaling. This thermocline shoaling, in turn, results in declining sea surface temperatures and increased surface
514 water productivity through the upwelling nutrient-rich thermocline waters along the Oman Margin during this time
515 (Fig. 3; Zhuang et al., 2017; Bialik et al., 2020a).

516 Declining high Mn/Al ratios and diverse nanofossil assemblages point towards a relatively low nutrient regime
517 between 15.0 and 13.5 Ma. Patterns of Mn decline have been observed since at least 15 Ma in the Maldives, which
518 is in line with observations at Site 722 (Betzler et al., 2016; Bialik et al., 2020a, b). This period thus represents a

519 progressive increase in upwelling intensity during the MMCT due to globally declining SSTs and sea levels
520 following the end of the MCO (Zhuang et al., 2017; Miller et al., 2020). Both nannoplankton and planktonic
521 foraminifera reflect primarily open marine, low-nutrient conditions (Sexton and Norris, 2011; Lessa et al., 2020).
522 By 13.5 Ma, these progressive changes culminate in a first sustained community shift in both nannofossil and
523 planktonic foraminifera records (Figs. 2 & 5).

524 We consider these shifts to be a coupled response of Site 722 phytoplankton communities to increased surface
525 water nutrient levels that subsequently allowed a population increase of heterotrophs such as foraminifera. These
526 changes are consistent with establishing a more pronounced upwelling regime, which also resulted in the expansion
527 of the OMZ further into the Indian Ocean, reaching the Maldives by ~13 Ma. Furthermore, available TOC data
528 still show low accumulation rates at Site 722 at this time, indicating that organic matter was still recycled mainly
529 within the expanding OMZ (Bialik et al., 2020a).

530 By ~12 Ma, another phytoplankton community shift (see interval 2b) leads to a size increase in the
531 reticulofenestrads, lower nannoplankton diversity, and a higher abundance of thermocline-dwelling planktonic
532 foraminifer taxa (Fig. 5). Together with increasing TOC fluxes (Fig. 3), all these shifts point towards increasing
533 productivity. These changes, however, happen without any significant changes in overall temperature within the
534 upwelling zone (Zhuang et al., 2017). A northward shift of the southern hemisphere westerlies is recorded by 12
535 Ma (Groeneveld et al., 2017). We hypothesize that this shift and a potential increase in wind strength may have
536 also increased nutrient concentrations in intermediate water masses within the sub-Antarctic frontal system. This
537 interpretation would be in line with the effect increasing sea ice cover would have had on intermediate water
538 nutrient concentrations based on modelling data and evidence from southern hemisphere records (Sarmiento et al.,
539 2004; Sarmiento and Gruber, 2013; Laufkötter and Gruber, 2018; Groeneveld et al., 2017). Such enhanced nutrient
540 transport within the thermocline would reconcile increased productivity without increasing the total volume of
541 upwelling – and consequently reducing SSTs - along the Oman Margin. The first occurrence of diatoms within
542 this interval may also point towards a shift in nutrient availability and increased phosphorus and silicon availability
543 within the upwelling cell and likely globally (Keller and Barron, 1983). Decreasing P- and Si-limitation would
544 thus provide more favourable conditions for highly efficient photosynthesizers, such as diatoms within the water
545 column (Schiebel et al., 2004; Brembu et al., 2017; Sarmiento and Gruber, 2013). Within the plankton community,
546 we also note the first intermittent occurrences of elevated *G. bulloides* abundances, indicative of high productivity
547 upwelling conditions (Kroon et al., 1991; Gupta et al., 2015).

548 By 11 Ma, global climatic shifts and further decreasing sea levels (Miller et al., 2020; Westerhold et al., 2020) led
549 to another step in the water masses upwelling in the WAS (Fig. 6). As a result of these water mass changes, diatoms
550 dominate our phytoplankton record by 11 Ma, outpacing nannoplankton for the first time, while we note a first
551 sustained occurrence (> 25 %) of *G. bulloides*. Therefore, we interpret this shift as the inception of sustained
552 primary productivity within the upper water column of an upwelling cell supplied with enough Si, as well as P and
553 N, to sustain a large diatom population (Brzezinski, 1985; Sarmiento and Gruber, 2013; Closset et al., 2021).

554 However, the abundance of discoasterids and sphenoliths within our nannofossil record (Fig. 5) still needs to be
555 reconciled with this interpretation. Both taxa are considered to be indicative of low nutrient conditions and
556 increased stratification (Gibbs et al., 2004a; Schueth and Bralower, 2015; Karatsolis and Henderiks, 2023). This
557 information is thus contrary to our recorded high abundances of mixed layer dwelling foraminifera and high
558 nutrient-adapted diatoms dominating the phytoplankton record. A possible way of integrating these opposite

559 requirements is to evoke a highly seasonal upwelling cell with strong upwelling in one season and calm and
560 stratified surface waters providing a deep thermo- and nutricline in the other.
561 This seasonal variability is most evident after 9.6 Ma when *Sphenolithus* abundances also increase together with
562 overall nannofossil diversity (Fig. 5, interval 3b). These changes in the nannofossil community are also associated
563 with decreasing diatom abundances and TOC fluxes while upwelling indicative planktonic foraminifera taxa
564 remain common. It thus seems that an initial spike in upwelling and, therefore, diatom accumulation waned again,
565 pointing towards a significant reorganization of the upwelling cell after 9.6 Ma.
566 Within the topmost three samples of the record, belonging to interval 4, we note an increase in small
567 reticulofenestrads corresponding to the base absence of *Reticulofenestra pseudoumbilicus* around 8.8 Ma,
568 according to accepted nannofossil biostratigraphy (Young, 1990; Backman et al., 2012; Imai et al., 2015). We note
569 that this significant size change and an increase in small placoliths are very pronounced within our WAS records
570 from Site 722, in agreement with Young (1990). While we cannot contribute to the discussion of whether this
571 assemblage shift constitutes an evolutionary-driven adaptation of taxa within the genus *Reticulofenestra* or purely
572 an ecophenotypically driven size adaption (Young, 1990; Imai et al., 2015). We still note that a clear link to
573 changing nutrient levels within the upwelling cell is becoming apparent. Imai et al. (2015) further hypothesized
574 that the size shift is related to nutrient increases within the Indo-Pacific. Based on our records of high nutrient
575 conditions and likely at least intermittent seasonal eutrophication persisting from at least 11 Ma, we cannot
576 completely follow their hypotheses that increasing nutrient levels within the surface ocean were the sole driver for
577 this size shift. Therefore, we propose that changing nutrient limitation within the mixed layer may have played an
578 important, as-of-yet unconsidered role in defining the predominant assemblage structure within the WAS
579 upwelling system during the Middle and Late Miocene (Fig. 7).

580 **5.4. Contextualizing the primary drivers for plankton community shifts**

581 The modern productivity patterns and oxygen depletion in the northwestern Indian Ocean differ significantly from
582 those observed in the studied period. For example, the increase in Mn content in the Maldives in the Pliocene
583 (Betzler et al., 2016) suggests a significant reduction in Mn redirection, which continued until today. This is indeed
584 visible in present-day oceanographic records, where elevated Mn concentrations are only found near the margins
585 of the Arabian Sea (ThiDieuVu and Sohrin, 2013). Meanwhile, denitrification in the Eastern Arabian Sea appears
586 to have only become significant during the Pliocene (Tripathi et al., 2017). These changes in productivity patterns
587 thus may indicate that the WAS was potentially more productive during the Late Miocene than today and
588 potentially even supported an expanded OMZ (Dickens and Owen, 1999, 1994).
589 Despite that, we note that even in the most productive parts of the Arabian Sea, conditions are rarely eutrophic
590 (Fig. 1a). As such, ascribing permanent eutrophic or even mesotrophic conditions to any of these assemblages is
591 unlikely to be reasonable. On the other hand, nannofossil assemblages such as TG 3 with combined diatom
592 occurrences possibly indicate the prevalence of mesotrophic and eutrophic conditions. Diatoms are generally less
593 adapted to low nutrient levels, requiring much higher P and N levels to form blooms compared to coccolithophores
594 (Hutchins and Bruland, 1998; Litchman et al., 2006). If enough nutrients (including Si) are available, they tend to
595 outcompete coccolithophores quickly and begin to dominate the mineralizing phytoplankton community (Schiebel
596 et al., 2004; Brzezinski, 1985; Closset et al., 2021). Based on modern analogs, it seems likely that shifts in the
597 nutrient content of upwelling waters may have played an important role in controlling the observed patterns in
598 the plankton community along the WAS during the Middle to Late Miocene. In particular after 13 Ma, where a

599 **stustained** and stable SAM **regieme** seems to have existed during the northern hemisphere summer (Betzler et al.,
600 2016). To disentangle these patterns we therefore focus on understanding observed patterns of the two dominant
601 phytoplankton groups present within our record, with the context of their ecological preferences and primary
602 nutrient requirements within our study interval.

603 The co-occurrence of diatoms, discoasterids, and sphenoliths in the upper part of the studied interval (Fig. 5) ~~thus~~
604 suggests that while nutrient levels were high, upwelling was likely highly seasonal. For the WAS, high seasonality
605 may be the result of strengthening summer monsoon winds with no changes in winter monsoon winds (Schiebel
606 et al., 2004; Rixen et al., 2019b; Sarr et al., 2022). Increasing summer but stable or absent winter monsoon
607 conditions are likely the result of increased cooling in the southern hemisphere (Bialik et al., 2020a; Gadgil, 2018;
608 Sarr et al., 2022). This asymmetric cooling strengthened the summer monsoon compared to the winter monsoon
609 system, which only intensified ~7 Ma (Gupta and Thomas, 2003; Holbourn et al., 2018; Rixen et al., 2019b).

610 The variability in wind and upwelling intensity and their interaction with nutrient availability, thus, likely also
611 affected the community structure and size variability of primary producers on longer geological time scales. The
612 community structure of primary producers then exerted control on first-level consumers, such as planktonic
613 foraminifera.

614 Upwelling-derived TOC accumulation, primary productivity assemblages, and upwelling indicative foraminifera
615 show distinctive patterns, which are, however, not in complete agreement with wind proxies and the suggested
616 expansion of the OMZ around 13 Ma (Betzler et al., 2016). These discrepancies resulted in a long-standing debate
617 about the validity and usefulness of upwelling proxies as monsoonal indicators (Betzler et al., 2016; Clift and
618 Webb, 2018; Bialik et al., 2020a; Yang et al., 2020; Sarr et al., 2022). We propose that this disagreement is
619 primarily due to inadequate treatment of nutrient limitation and nutrient supply in conjunction with wind speed
620 when evaluating primary productivity in the WAS (Fig. 5, 7).

621 Modern-day upwelling zones in the low-to-mid-latitudes are generally well supplied in macro-nutrients, resulting
622 in iron-limited environments or other micro- and nano-nutrient limitations (Moore et al., 2013). However,
623 currently, the fringing areas of upwelling zones are commonly N-limited through increased denitrification in
624 underlying OMZs (Moore et al., 2013; Bristow et al., 2017; Anju et al., 2020; Buchanan et al., 2021; Ustick et al.,
625 2021; Buttay et al., 2022). Within the WAS upwelling zone, major nutrients N, P, and to some degree, minor
626 nutrients such as Si are replenished through local recycling and intermixing with deep and intermediate water
627 masses originating from Antarctica (Fig. 7; Sarmiento et al., 2004; Meisel et al., 2011; Sarmiento and Gruber,
628 2013; Laufkötter and Gruber, 2018). Iron, a key micronutrient, is primarily supplied through dust and riverine
629 influxes from surrounding continental sources (Kunkelova et al., 2022; Moore et al., 2013; Guieu et al., 2019).

630 Accepting that the wind regime had reached peak intensity by 13 Ma following a gradual increase from the end of
631 the MCO (Betzler et al., 2016, 2018), the significant increase in diatom abundance and TOC accumulation after
632 12 Ma is not contemporary. Therefore, the availability of nutrients and the nutrient composition also played a key
633 role in defining the variability between coccolithophore and diatom abundances within the WAS upwelling cell.
634 Moreover, the shift in the reticulofenestrid morphotypes (Fig. 5) may also be linked to the state of nutrient
635 limitation. Paasche (1998) also has shown that modern-day coccolithophores tend to increase the formation of
636 small placoliths during N-limitation.

637 Therefore, the shift towards higher primary productivity after 12 Ma, **including first record** of diatoms at Site 722,
638 may indicate a change in nutrient composition along the WAS without necessitating a change in **monsson** wind
639 strength. Notably, during this time, the northward expansion of the southern hemisphere westerlies shifted the

640 position of the polar and sub-Antarctic frontal system (Fig 6). In particular, the Late Miocene sea ice expansion
641 after 11 Ma strongly affected the Antarctic frontal system and, in turn, the nutrient enrichment of intermediate
642 waters formed in this region (Groeneveld et al., 2017; Bijl et al., 2018; Laufkötter and Gruber, 2018). Here we
643 propose that changes in the mode of intermediate water formation significantly increased the nutrient availability
644 in intermediate waters in the Antarctic frontal system, resulting in modern-like downwelling dynamics around
645 Antarctica (Fig. 7). Furthermore, many modeling studies support the assumption that climatic changes affecting
646 the Antarctic frontal system can strongly influence global productivity patterns (Sarmiento et al., 2004; Laufkötter
647 and Gruber, 2018; Moore et al., 2018; Taucher et al., 2022). We, therefore, propose that the Middle to Late
648 Miocene productivity changes in the WAS offer compelling evidence for this hypothesis.

649 **5.5. Synthesizing Miocene nutrient transport and monsoonal upwelling**

650 Thus far, the discussion was focused on local aspects of the record in Site 722 in the WAS and northwestern Indian
651 Ocean. However, the interconnected nature of the oceanic circulation and nutrient rejuvenation system means that
652 critical mechanisms may be overlooked without a global perspective. For example, modeling evidence for nutrient
653 transport and nutrient enrichment in low-latitude upwelling cells allows for the construction of a timeline of
654 changes along the WAS and their interaction with plankton communities. Moreover, a complete oceanic
655 perspective allows for contextualization into the broader evolution of the ocean-atmosphere system.

656 Initial plankton community structures agree with a generally low nutrient regime in a somewhat muted wind
657 regime, based on a large amount of deep thermocline dwelling taxa in the foraminifera community, likely
658 following the dominant phytoplankton primary productivity in the deeper photic zone (Lessa et al., 2020). In
659 addition, the mixed layer is dominated by a diverse nannofossil assemblage (H' -diversity of around 1.5 within
660 intervals 1 and 2). During the MMCT, wind shear strengthened by 13 Ma, resulting in a significant global shift in
661 ocean-atmospheric circulation exemplified in the global reorganization of carbonate-platform geometries and
662 thermocline deepening and ventilation at Site 722, as shown by the increase in mixed-layer dwelling planktonic
663 foraminifera (Betzler et al., 2016, 2018; Betzler and Eberli, 2019; Lessa et al., 2020).

664 Modeling studies for the WAS link the initial intensification of upwelling and wind shear to a combination of
665 increased latitudinal temperature gradients and the emergence of the Arabian Peninsula during the Middle Miocene
666 (Zhang et al., 2014; Sarr et al., 2022; Yang et al., 2020). Notably, while OMZ expansion and Mn redirection are
667 evident since at least ~14 Ma at Site 722 (Bialik et al., 2020a), available productivity records support at most
668 intermittently mesotrophic and likely P- and N-limited conditions before ~12 Ma (Fig. 5). We thus propose that
669 the upwelling cell in the WAS was wholly influenced by strong post-MMCT winds by 13 Ma. Productivity was
670 still limited by the upwelling of comparably low nutrient intermediate waters of local origin (Fig. 7). Likely
671 originating in the marginal seas of the northwestern Indian Ocean, these water masses may have been remnants of
672 the Tethyan Intermediate Water (TIW). While the Tethyan Seaway had terminated between 14 and 15 Ma (Bialik
673 et al., 2019), TIW or a similar high salinity mass (Woodruff and Savin, 1989; Smart et al., 2007) was still affecting
674 the Northern Indian Ocean until at least 12 Ma. This remnant TIW can be considered a more potent form of the
675 modern Red Sea and Persian Gulf Intermediate Waters (RSPGW; Fig 7). These warm and salty intermediate waters
676 may have played a much more substantial role in the WAS during the early stages of the uplift of the Arabian
677 Peninsula (Woodruff and Savin, 1989; Tomczak and Godfrey, 2003; Chowdary et al., 2005; Smart et al., 2007;
678 Acharya and Panigrahi, 2016). The influence of remnant TIW would also align with the high abundance of

679 thermocline-dwelling taxa until 12 Ma, which we infer to be representative of a shallow and/or a poorly ventilated
680 thermocline (Sexton and Norris, 2011; Lessa et al., 2020).

681 It thus seems likely that late Middle Miocene WAS upwelling may have been relatively nutrient-poor. We
682 speculate that these water masses may have suppressed primary productivity, muting the influence of the
683 increasing Findlater Jets and the emerging Arabian Peninsula (e.g., Sarr et al., 2022) compared to today. Invoking
684 significant TIW upwelling until at least 12 Ma would further reconcile the discrepancy between the occurrence of
685 drift deposits in the Maldives, and thus strong monsoon winds and the first clear evidence for strong upwelling in
686 the WAS, with the abundance increase of upwelling indicative planktonic foraminifera (e.g., *G. bulloides*; Fig 5)
687 and the first occurrence of diatoms at Site 722 (Fig 5; Kroon et al., 1991; Huang et al., 2007b; Gupta et al., 2015;
688 Bialik et al., 2020a). This change in nutrient availability is also reflected by a contemporary increase in medium-
689 sized reticulofenestrads (*R. antarctica* and *R. haqii*), which are generally assumed to reflect higher nutrient
690 availability due to upwelling (Fig. 5; Auer et al., 2019 and references therein).

691 Productivity in the WAS thereby only began to increase as remnant TIW got progressively supplanted by other,
692 more nutrient-rich, water masses. At present, the waters upwelling in the Arabian Sea is primarily regarded to be
693 ICW, which therefore also includes IOW, SAMW and AAIW (You, 1997, 1998; Böning and Bard, 2009; Munz et
694 al., 2017; Chinni and Singh, 2022). Today AAIW and SAMW forming in the northern branch of the Antarctic
695 Divergence, control up to 75% of low-latitude productivity (Sarmiento et al., 2004). We hypothesize that the
696 increasing formation of AAIW and SAMW following the northward shift of the westerlies around 12 Ma (Fig.6)
697 may have modulated low latitude productivity (Groeneveld et al., 2017; Laufkötter and Gruber, 2018; Moore et
698 al., 2018; Taucher et al., 2022). This time also aligns well with the proposed inception of the northward shift of
699 southern hemisphere climate belts and the invigoration of the south equatorial current (LeHouedec et al., 2012;
700 Reuter et al., 2019). Following that, it can also be assumed that by 12 Ma, the northward expansion of the southern
701 hemisphere Westerlies resulted in a near-modern Antarctic Divergence (Groeneveld et al., 2017; Laufkötter and
702 Gruber, 2018).

703 This global change in circulation patterns was fully established by 11 Ma, with cool nutrient-rich SAMW/AAIW
704 waters reaching Site 722, evidenced by a further SST drop (Zhuang et al., 2017). This resulted in the highest
705 productivity in the WAS upwelling cell during the Miocene (Figs. 5-7). The Late Miocene high-productivity
706 interval in the WAS, is thus the result of intense summer monsoon-dominated AAIW/SAMW upwelling, fueled
707 by the Findlater Jets and forced by steep latitudinal temperature gradients and favourable tectonic conditions on
708 the Arabian Peninsula (Pound et al., 2012; Zhang et al., 2014; Sarr et al., 2022). Summer months were thus
709 characterized by eutrophic P-, N-, and potentially Si-enriched waters, allowing the proliferation of diatoms and
710 other siliceous organisms. Winter months, in contrast, favoured the accumulation of deep-dwelling discoasterids
711 that utilized the nutrient-rich waters below a relatively deeper winter thermocline. Higher abundances of mixed-
712 layer dwelling taxa also reflect the increased mixed-layer depth (Fig. 5). Expanding AAIW/SAMW-fueled high
713 productivity that consequently also resulted in the highest recorded TOC fluxes between 11 – 10 Ma and a
714 substantial OMZ expansion deep into the equatorial Indian Ocean (Dickens and Owen, 1994; Bialik et al., 2020a).
715 Increasing OMZs also resulted in a global increase in denitrification, which is well-recorded in foraminifer-bound
716 $\delta^{15}\text{N}$ records, showing a trend from more oxygenated intermediate waters during the MCO to lower oxygenated
717 waters in the Late Miocene in the Indo-Pacific (Auderset et al., 2022).

718 By 10 Ma, OMZs had reached a critical threshold, leading to another substantial change in nutrient conditions
719 within the WAS upwelling. Through increased denitrification in the OMZ underlying the upwelling cell, nitrate

720 and ammonia were lost through bacterial conversion to N₂ (Sigman and Fripiat, 2019). Strong denitrification
721 subsequently led to increasingly N-limited water masses upwelling within the WAS. Although concrete evidence
722 is only presented for the WAS, these patterns could also have occurred globally, considering the clear evidence
723 for decreasing ocean oxygenation during the Late Miocene (Auderset et al., 2022). The Late Miocene N-limitation
724 in the WAS upwelling cell is chiefly expressed by a decline in diatom abundances after 10 Ma, in conjunction with
725 overall community shifts in the nannofossil assemblage.

726 Total upwelling intensity also remained consistently high, as indicated by the available SST record of Zhuang et
727 al. (2017). Primary productivity thus remained relatively high, which is characterized by the continued presence
728 and even dominance of large reticulofenestrads, diatoms, and the continuously high TOC concentration within the
729 sediment (often > 1 wt.%; Fig. 3). We thus assume that the drop in diatom abundance and intermittent decline in
730 $\delta^{15}\text{N}$ values at Site 722 (Figs. 3, 5.) were not caused by decreasing upwelling intensity but rather a decline in P and
731 Si availability and, thus declining export of diatom-derived organic matter. The increase in sphenoliths within our
732 Site 722 record (Fig. 5) could indicate increased environmental stress within the nannofossil assemblage (Wade
733 and Bown, 2006). Sphenoliths are likely not a good indicator of long-term stratification changes (Karatsolis and
734 Henderiks, 2023) in highly seasonal upwelling regimes like the WAS, as high TOC and thus sustained, but lower,
735 diatom fluxes indicate continued upwelling after 10 Ma at Site 722. Sustained seasonal upwelling and high organic
736 matter export (Fig. 3) are further inferred by decreasing organic carbon $\delta^{13}\text{C}$ throughout this interval (Bialik et al.,
737 2020a and references therein).

738 By 8.8 Ma, the adaption of smaller reticulofenestrads may result in an evolutionary adaption to the continued N-
739 limited nutrient availability in the WAS. We base this interpretation on the nutrient adaption of coccolithophorids
740 based on modern culture experiments (Paasche, 1998). Although somewhat anecdotal, these offer the currently
741 best explanation to reconcile the recorded history of Site 722 upwelling changes with the stark shifts in
742 reticulofenestrads size ranges. It should be noted that these shifts have been recorded throughout the mid- and low
743 latitudes of the Indopacific (Young, 1990; Imai et al., 2015). However, the full impact of this hypothesis needs to
744 be tested further.

745 The data compilation of Young (1990) further shows that the recorded Late Miocene size shift was primarily
746 limited to the low and mid-latitudes, with larger reticulofenestrads persisting within in the higher latitudes. We
747 propose that the transition in *Reticulofenestra* morphology from large to small morphotypes thus primarily
748 represents a significant shift in nutrient limitation rather than total nutrient availability within the mid to low
749 latitudes. We further argue that this turnover reflects N-limitation within the low- and mid-latitudes due to
750 sustained and intense denitrification after 12 Ma (Auderset et al., 2022). Further studies, particularly on
751 ultrastructural morphotaxonomy of reticulofenestrads, will be needed to fully disentangle the implications of the
752 proposed N-limited nanno-floral turnover.

753 The highly opportunistic small *Reticulofenestra* morphotype was subsequently also able to sustain phytoplankton
754 blooms in the WAS, as evidenced by the significant increase in nannofossils within the sediment (Fig. 5).
755 Furthermore, the high mass of small coccolith cells potentially also contributed to the re-establishment of strong
756 denitrification as evidenced by a rise in $\delta^{15}\text{N}$ -values after 8.8 Ma (Fig. 3), as their additional biomass contributed
757 to OMZ re-expansion. Detailed records of Late Miocene OMZ strength throughout the Indian Ocean will, however,
758 be necessary to fully quantify the impact on local upwelling. Local tectonics also began to modify the region
759 configuration at this time (Rodriguez et al., 2014), leading to bottom current intensification (Rodriguez et al.,
760 2016), which may have also modulated subsequent OMZ dynamics (Dickens and Owen, 1999).

761 **6. Conclusions**

762 We present fully quantitative nannofossil and planktonic foraminifera assemblage data in conjunction with diatom
763 frustule abundances for Site 722. Within a multi-proxy framework, these novel data allowed us to disentangle the
764 complex and long-debated changes within the upwelling system of the WAS in the Middle to Late Miocene. We
765 show that the Findlater Jets, and thus Indian summer monsoon wind strength, are the primary drivers of upwelling.
766 However, wind-driven upwelling is also clearly modulated by local and global water mass changes and changing
767 nutrient fluxes. In particular, changing nutrient transport through intermediate waters has had a significant – until
768 now unconsidered – impact on primary productivity patterns and plankton communities over the Middle and Late
769 Miocene in the Indian Ocean. We, therefore, reach the following key conclusion:

770 (1) the expansion and evolution of upwelling within the WAS as a complex interplay of regional tectonics, global
771 climate, and ice volume changes affected upwelling intensity and nutrient availability. The present study
772 emphasizes that wind and nutrient changes are intrinsically related but do not necessarily operate in tandem on
773 longer supra-Milankovitch time scales. It is, therefore, crucial to consider both water mass changes and
774 atmospheric conditions when investigating past wind-driven upwelling regimes.

775 (2) The interaction first invigorated monsoonal circulation after the MMCT before resulting in the reorganization
776 of intermediate water circulation, controlled by the inception of a near-modern configuration of the Antarctic
777 Divergence, which supplied nutrient rich intermediate waters to the low latitudes.

778 (3) These processes led to the progressive establishment of near-modern nutrient transport within the Indian Ocean
779 by 12 to 11 Ma. Furthermore, these changes acted together with denitrification in expanding global OMZs
780 (Auderset et al., 2022) to increase N-limitation and subsequent adaption of coccolithophorids to the new nutrient
781 conditions in the mid to low latitudes.

782 (4) We provide a timeline of events that agrees with global climatic and local productivity patterns, which are all
783 linked through the invigoration of upwelling cells and nutrient fluxes through intermediate water masses into the
784 lower latitudes. In particular past changes in intermediate water mass circulation, replenishment, and expansion
785 appear to be a key – and critically understudied – aspect within paleoceanography and paleoclimatology that is
786 crucial to understanding past and, thereby, future low latitude productivity.

787 **7. Data and code availability**

788 Data and code are available from the supplementary material and on Pangaea (DOI: will be provided once
789 available).

790 **8. Author contribution**

791 **GA:** designed the study, acquired funding, conducted nannofossil counts and statistics, wrote the first draft, edited
792 the text, and drafted the figures. **OMB:** designed the study, performed statistical analyses, wrote the first draft,
793 edited the text, and helped draft the figures. **MEA:** performed planktonic foraminifera taxonomic analysis and
794 assemblage interpretation and contributed to the first draft of the text. **NVV:** helped draft the figures and
795 contributed to data interpretation, edited the final draft of the MS. **WEP:** supervised and conducted foraminiferal
796 analysis and contributed to writing and editing of the text.

797 **9. Competing interests**

798 The authors declare that they have no conflict of interest.

799 **10. Acknowledgments**

800 This research used samples and data provided by the Ocean Drilling Program (ODP) and the International Ocean
801 Discovery Program (IODP). This study was funded by the Austrian Science Fund (FWF Project P36046-N;
802 MIO:TRANS – Nutrient Fluxes in the Miocene Indian Ocean). OMB is partially supported by the German
803 (GEOMAR)-Israeli (University of Haifa) Helmholtz International Laboratory -The Eastern Mediterranean Sea
804 Centre- An Early-Warning Model-System for our Future Oceans: EMS Future Ocean Research (EMS FORE).
805 Furthermore, the authors would like to thank all Bialik et al. (2020) authors for their invaluable contribution to this
806 research and their expertise in interpreting the data. In particular, we would like to thank Dick Kroon for his early
807 support of these studies and his invaluable discussions on the subject matter.

809

810 Acharya, S. S. and Panigrahi, M. K.: Eastward shift and maintenance of Arabian Sea oxygen
811 minimum zone: Understanding the paradox, *Deep Sea Res. Part I Oceanogr. Res. Pap.*, 115,
812 240–252, <https://doi.org/10.1016/j.dsr.2016.07.004>, 2016.

813 Agnini, C., Monechi, S., and Raffi, I.: Calcareous nannofossil biostratigraphy: historical
814 background and application in Cenozoic chronostratigraphy, *Lethaia*, 50, 447–463,
815 <https://doi.org/10.1111/let.12218>, 2017.

816 Alam, M., Tripti, M., Gurumurthy, G. P., Sohrin, Y., Tsujisaka, M., Singh, A. D., Takano, S.,
817 and Verma, K.: Palaeoredox reconstruction in the eastern Arabian Sea since the late Miocene:
818 Insights from trace elements and stable isotopes of molybdenum ($\delta^{98/95}\text{Mo}$) and tungsten
819 ($\delta^{186/184}\text{W}$) at IODP Site U1457 of Laxmi Basin, *Palaeogeogr Palaeoclim Palaeoecol*, 587,
820 110790, <https://doi.org/10.1016/j.palaeo.2021.110790>, 2022.

821 Anju, M., Sreeush, M. G., Valsala, V., Smitha, B. R., Hamza, F., Bharathi, G., and Naidu, C.
822 V.: Understanding the Role of Nutrient Limitation on Plankton Biomass Over Arabian Sea
823 Via 1-D Coupled Biogeochemical Model and Bio-Argo Observations, *J Geophys Res Oceans*,
824 125, <https://doi.org/10.1029/2019jc015502>, 2020.

825 Aubry, M.-P.: *Handbook of Cenozoic Calcareous Nannoplankton: Book 1. Ortholithae*
826 *(Discoasters)*, Micropaleontology Press, 1984.

827 Aubry, M.-P.: *Handbook of Cenozoic Calcareous Nannoplankton: Book 2. Ortholithae*
828 *(Holococcoliths, Ceratoliths, Ortholiths and Others)*, Micropaleontology Press, 1988.

829 Aubry, M.-P.: *Handbook of Cenozoic Calcareous Nannoplankton: Book 3. Ortholithae*
830 *(Pentaliths, and Others), Heliolithae (Fasciculiths, Sphenoliths and Others)*,
831 Micropaleontology Press, 1989.

832 Aubry, M.-P.: *Handbook of Cenozoic Calcareous Nannoplankton: Book 4. Heliolithae*
833 *(Helicoliths, Cribriliths, Lopadoliths and Others)*, Micropaleontology Press, 1990.

834 Aubry, M.-P.: *Handbook of Cenozoic Calcareous Nannoplankton. Book 5: Heliolithae*
835 *(Zygoliths and Rhabdoliths)*, Micropaleontology Press, 1999.

836 Aubry, M.-P.: A major Pliocene coccolithophore turnover: Change in morphological strategy
837 in the photic zone, vol. 424, *Geological Society of America*, 25–51,
838 [https://doi.org/10.1130/2007.2424\(02\)](https://doi.org/10.1130/2007.2424(02)), 2007.

839 Aubry, M.-P.: *Coccolithophores: Cenozoic Discoasterales—Biology, Taxonomy,*
840 *Stratigraphy*, 460 pp., 2021.

841 Auderset, A., Moretti, S., Taphorn, B., Ebner, P.-R., Kast, E., Wang, X. T., Schiebel, R.,
842 Sigman, D. M., Haug, G. H., and Martínez-García, A.: Enhanced ocean oxygenation during
843 Cenozoic warm periods, *Nature*, 609, 77–82, <https://doi.org/10.1038/s41586-022-05017-0>,
844 2022.

845 Auer, G., Piller, W. E., and Harzhauser, M.: High-resolution calcareous nannoplankton
846 palaeoecology as a proxy for small-scale environmental changes in the Early Miocene, *Mar.*
847 *Micropaleontol.*, 111, 53–65, <https://doi.org/10.1016/j.marmicro.2014.06.005>, 2014.

848 Auer, G., Piller, W. E., and Harzhauser, M.: Two distinct decadal and centennial cyclicities
849 forced marine upwelling intensity and precipitation during the late Early Miocene in central
850 Europe, *Clim. Past.*, 11, 283–303, <https://doi.org/10.5194/cp-11-283-2015>, 2015.

851 Auer, G., DeVleeschouwer, D., Smith, R. A., Bogus, K., Groeneveld, J., Grunert, P.,
852 Castañeda, I. S., Petrick, B., Christensen, B., Fulthorpe, C., Gallagher, S. J., and Henderiks,
853 J.: Timing and Pacing of Indonesian Throughflow Restriction and Its Connection to Late
854 Pliocene Climate Shifts, *Paleoceanogr. Paleoclimatol.*, 34, 635–657,
855 <https://doi.org/10.1029/2018pa003512>, 2019.

856 Avinash, K., Manjunath, B. R., and Kurian, P. J.: Glacial-interglacial productivity contrasts
857 along the eastern Arabian Sea: Dominance of convective mixing over upwelling, *Geosci*
858 *Front.*, 6, 913–925, <https://doi.org/10.1016/j.gsf.2015.03.003>, 2015.

859 Aze, T., Ezard, T. H. G., Purvis, A., Coxall, H. K., Stewart, D. R. M., Wade, B. S., and
860 Pearson, P. N.: A phylogeny of Cenozoic macroperforate planktonic foraminifera from fossil
861 data, *Biol Rev.*, 86, 900–927, <https://doi.org/10.1111/j.1469-185x.2011.00178.x>, 2011.

862 Backman, J., Raffi, I., Rio, D., Fornaciari, E., and Pälke, H.: Biozonation and biochronology
863 of Miocene through Pleistocene calcareous nannofossils from low and middle latitudes,
864 *Newsl. Stratigr.*, 45, 221–244, <https://doi.org/10.1127/0078-0421/2012/0022>, 2012.

865 Backman, J., Raffi, I., Ciummelli, M., and Baldauf, J.: Species-specific responses of late
866 Miocene *Discoaster* spp. to enhanced biosilica productivity conditions in the equatorial
867 Pacific and the Mediterranean, *Geo-mar Lett.*, 33, 285–298, <https://doi.org/10.1007/s00367-013-0328-0>, 2013.

869 Baldauf, J. G., Barron, J. A., Ehrmann, W. U., Hempel, P., and Murray, D.: Synthesis of
870 Results from Scientific Drilling in the Indian Ocean, *Geophys Monogr Ser.*, 70, 335–349,
871 <https://doi.org/10.1029/gm070p0335>, 1992.

872 Balun, A., Field, D. B., Redondo-Rodriguez, A., and Weeks, S. J.: Greenhouse gas,
873 upwelling-favorable winds, and the future of coastal ocean upwelling ecosystems, *Global*
874 *Change Biol.*, 16, 1213–1228, <https://doi.org/10.1111/j.1365-2486.2009.02094.x>, 2010.

875 Basavani, P.: Findlater Jet Climatology in Summer Monsoon Its Role on Onset Progress and
876 Relation with Air Sea Interaction Parameters Over Arabian Sea, 2013.

877 Beltran, C., Rousselle, G., Backman, J., Wade, B. S., and Sicre, M.-A.: Paleoenvironmental
878 conditions for the development of calcareous nannofossil acme during the late Miocene in the
879 eastern equatorial Pacific, *Paleoceanography*, 29, 210–222,
880 <https://doi.org/10.1002/2013pa002506>, 2014.

881 Berggren, W. A., Kennett, J. P., and Srinivasan, M. S.: Neogene Planktonic Foraminifera: A
882 Phylogenetic Atlas, *Micropaleontology*, 31, 94, <https://doi.org/10.2307/1485586>, 1985.

- 883 Betzler, C. and Eberli, G. P.: Miocene start of modern carbonate platforms, *Geology*, 47, 771–
884 775, <https://doi.org/10.1130/g45994.1>, 2019.
- 885 Betzler, C., Eberli, G. P., Kroon, D., Wright, J. D., Swart, P. K., Nath, B. N., Alvarez-
886 Zarikian, C. A., Alonso-García, M., Bialik, O. M., Blättler, C. L., Guo, J. A., Haffen, S.,
887 Horozal, S., Inoue, M., Jovane, L., Lanci, L., Laya, J. C., Mee, A. L. H., Lüdmann, T.,
888 Nakakuni, M., Niino, K., Petruny, L. M., Pratiwi, S. D., Reijmer, J. J. G., Reolid, J., Slagle,
889 A. L., Sloss, C. R., Su, X., Yao, Z., and Young, J. R.: The abrupt onset of the modern South
890 Asian Monsoon winds., *Sci. Rep.*, 6, 29838, <https://doi.org/10.1038/srep29838>, 2016.
- 891 Betzler, C., Eberli, G. P., Lüdmann, T., Reolid, J., Kroon, D., Reijmer, J. J. G., Swart, P. K.,
892 Wright, J., Young, J. R., Alvarez-Zarikian, C., Alonso-García, M., Bialik, O. M., Blättler, C.
893 L., Guo, J. A., Haffen, S., Horozal, S., Inoue, M., Jovane, L., Lanci, L., Laya, J. C., Mee, A.
894 L. H., Nakakuni, M., Nath, B. N., Niino, K., Petruny, L. M., Pratiwi, S. D., Slagle, A. L.,
895 Sloss, C. R., Su, X., and Yao, Z.: Refinement of Miocene sea level and monsoon events from
896 the sedimentary archive of the Maldives (Indian Ocean), *Prog Earth Planet Sci*, 5, 5,
897 <https://doi.org/10.1186/s40645-018-0165-x>, 2018.
- 898 Bialik, O. M., Frank, M., Betzler, C., Zammit, R., and Waldmann, N. D.: Two-step closure of
899 the Miocene Indian Ocean Gateway to the Mediterranean, *Sci. Rep.*, 9, 8842–8852,
900 <https://doi.org/10.1038/s41598-019-45308-7>, 2019.
- 901 Bialik, O. M., Auer, G., Ogawa, N. O., Kroon, D., Waldmann, N. D., and Ohkouchi, N.:
902 Monsoons, Upwelling, and the Deoxygenation of the Northwestern Indian Ocean in Response
903 to Middle to Late Miocene Global Climatic Shifts, *Paleoceanogr. Paleoclimatol.*, 35,
904 <https://doi.org/10.1029/2019pa003762>, 2020a.
- 905 Bialik, O. M., Reolid, J., Betzler, C., Eberli, G. P., and Waldmann, N. D.: Source shifts to
906 periplatform deposits during the early to middle Miocene in response to climatic and
907 oceanographic forcing, Maldives, western Indian Ocean, *Palaeogeogr Palaeoclim Palaeoecol*,
908 559, 109969, <https://doi.org/10.1016/j.palaeo.2020.109969>, 2020b.
- 909 Bialik, O. M., Jarochovska, E., and Grossowicz, M.: Ordination analysis in sedimentology,
910 geochemistry and palaeoenvironment—Background, current trends and recommendations,
911 *Depositional Rec*, 7, 541–563, <https://doi.org/10.1002/dep2.161>, 2021.
- 912 Bijl, P. K., Houben, A. J. P., Hartman, J. D., Pross, J., Salabarnada, A., Escutia, C., and
913 Sangiorgi, F.: Paleoceanography and ice sheet variability offshore Wilkes Land, Antarctica –
914 Part 2: Insights from Oligocene–Miocene dinoflagellate cyst assemblages, *Clim. Past.*, 14,
915 1015–1033, <https://doi.org/10.5194/cp-14-1015-2018>, 2018.
- 916 Blain, S., Leynaert, A., Tréguer, P., Chretiennot-Dinet, M.-J., and Rodier, M.: Biomass,
917 growth rates and limitation of Equatorial Pacific diatoms, *Deep Sea Res Part Oceanogr Res*
918 *Pap*, 44, 1255–1275, [https://doi.org/10.1016/s0967-0637\(97\)00014-9](https://doi.org/10.1016/s0967-0637(97)00014-9), 1997.
- 919 Blanc-Valleron, M. M., Pierre, C., Caulet, J. P., Caruso, A., Rouchy, J. M., Cespuglio, G.,
920 Sprovieri, R., Pestrea, S., and Stefano, E. D.: Sedimentary, stable isotope and
921 micropaleontological records of paleoceanographic change in the Messinian Tripoli
922 Formation (Sicily, Italy), *Palaeogeogr. Palaeoclimatol. Palaeoecol.*, 185, 255–286,
923 [https://doi.org/10.1016/s0031-0182\(02\)00302-4](https://doi.org/10.1016/s0031-0182(02)00302-4), 2002.

- 924 Boersma, A. and Mikkelsen, N.: Miocene-Age Primary Productivity Episodes and Oxygen
 925 Minima in the Central Equatorial Indian Ocean, in: Proceedings of the Ocean Drilling
 926 Program, Scientific Results, Vol. 115, vol. 115, edited by: Duncan, R. A., Backman, and
 927 Peterson, L. C., <https://doi.org/10.2973/odp.proc.sr.115.162.1991>, 1990.
- 928 Bollmann, J.: Morphology and biogeography of Gephyrocapsa coccoliths in Holocene
 929 sediments, *Mar. Micropaleontol.*, 29, 319–350, [https://doi.org/10.1016/s0377-8398\(96\)00028-](https://doi.org/10.1016/s0377-8398(96)00028-x)
 930 [x](https://doi.org/10.1016/s0377-8398(96)00028-x), 1997.
- 931 Böning, P. and Bard, E.: Millennial/centennial-scale thermocline ventilation changes in the
 932 Indian Ocean as reflected by aragonite preservation and geochemical variations in Arabian
 933 Sea sediments, *Geochim. Cosmochim. Acta*, 73, 6771–6788,
 934 <https://doi.org/10.1016/j.gca.2009.08.028>, 2009.
- 935 Bordiga, M., Bartol, M., and Henderiks, J.: Absolute nannofossil abundance estimates:
 936 Quantifying the pros and cons of different techniques, *Rev. de Micropaleontol.*, 58, 155–165,
 937 <https://doi.org/10.1016/j.revmic.2015.05.002>, 2015.
- 938 Brembu, T., Mühlroth, A., Alipanah, L., and Bones, A. M.: The effects of phosphorus
 939 limitation on carbon metabolism in diatoms, *Philosophical Transactions Royal Soc B*
 940 *Biological Sci*, 372, 20160406, <https://doi.org/10.1098/rstb.2016.0406>, 2017.
- 941 Bristow, L. A., Mohr, W., Ahmerkamp, S., and Kuypers, M. M. M.: Nutrients that limit
 942 growth in the ocean, *Curr Biol*, 27, R474–R478, <https://doi.org/10.1016/j.cub.2017.03.030>,
 943 2017.
- 944 Brummer, G.-J. A. and Kučera, M.: Taxonomic review of living planktonic foraminifera, *J*
 945 *Micropalaeontol*, 41, 29–74, <https://doi.org/10.5194/jm-41-29-2022>, 2022.
- 946 Brzezinski, M. A.: The Si: C: N ratio of marine diatoms: interspecific variability and the
 947 effect of some environmental variables 1, *J. Phycol.*, 21, 347–357,
 948 <https://doi.org/10.1111/j.0022-3646.1985.00347.x>, 1985.
- 949 Buchanan, P. J., Aumont, O., Bopp, L., Mahaffey, C., and Tagliabue, A.: Impact of
 950 intensifying nitrogen limitation on ocean net primary production is fingerprinted by nitrogen
 951 isotopes, *Nat. Commun.*, 12, 6214, <https://doi.org/10.1038/s41467-021-26552-w>, 2021.
- 952 Buttay, L., Vasseur, D. A., González-Quirós, R., and Nogueira, E.: Nutrient limitation can
 953 explain a rapid transition to synchrony in an upwelling-driven diatom community, *Limnol*
 954 *Oceanogr*, 67, S298–S311, <https://doi.org/10.1002/lno.12033>, 2022.
- 955 Cao, W., Zahirovic, S., Flament, N., Williams, S., Golonka, J., and Müller, R. D.: Improving
 956 global paleogeography since the late Paleozoic using paleobiology, *Biogeosciences*, 14,
 957 5425–5439, <https://doi.org/10.5194/bg-14-5425-2017>, 2017.
- 958 Carlson, R. E.: A trophic state index for lakes, *Limnol Oceanogr*, 22, 361–369,
 959 <https://doi.org/10.4319/lo.1977.22.2.0361>, 1977.
- 960 Castradori, D.: Calcareous nannofossils in the basal Zanclean of the Eastern Mediterranean
 961 Sea: remarks on paleoceanography and sapropel formation, in: Proceedings of the Ocean

- 962 Drilling Program, 160 Scientific Results, vol. 160,
963 <https://doi.org/10.2973/odp.proc.sr.160.005.1998>, 1998.
- 964 Chaisson, W. P. and Ravelo, A. C.: Changes in upper water-column structure at Site 925, late
965 Miocene–Pleistocene: planktonic foraminifer assemblage and isotopic evidence, in:
966 Proceedings of the Ocean Drilling Program, 154 Scientific Results,
967 <https://doi.org/10.2973/odp.proc.sr.154.105.1997>, 1997.
- 968 Chinni, V. and Singh, S. K.: Dissolved iron cycling in the Arabian Sea and sub-tropical gyre
969 region of the Indian Ocean, *Geochim Cosmochim Acta*, 317, 325–348,
970 <https://doi.org/10.1016/j.gca.2021.10.026>, 2022.
- 971 Chowdary, J. S., Gnanaseelan, C., Thompson, B., and Salvekar, P. S.: Water mass properties
972 and transports in the Arabian Sea from Argo observations, *J. Atmos. Sci.*, 10, 235–260,
973 <https://doi.org/10.1080/17417530600752825>, 2005.
- 974 Clarke, K. R.: Non-parametric multivariate analyses of changes in community structure,
975 *Australian Journal of Ecology*, 18, 117–143, <https://doi.org/10.1111/j.1442-9993.1993.tb00438.x>, 1993.
- 977 Clift, P. D. and Webb, A. A. G.: A history of the Asian monsoon and its interactions with
978 solid Earth tectonics in Cenozoic South Asia, Geological Society, London, Special
979 Publications, SP483.1, <https://doi.org/10.1144/sp483.1>, 2018.
- 980 Closset, I., McNair, H. M., Brzezinski, M. A., Krause, J. W., Thamatrakoln, K., and Jones, J.
981 L.: Diatom response to alterations in upwelling and nutrient dynamics associated with climate
982 forcing in the California Current System, *Limnol Oceanogr*, 66, 1578–1593,
983 <https://doi.org/10.1002/lno.11705>, 2021.
- 984 Cullen, J. J.: Hypotheses to explain high-nutrient conditions in the open sea, *Limnol*
985 *Oceanogr*, 36, 1578–1599, <https://doi.org/10.4319/lo.1991.36.8.1578>, 1991.
- 986 Dickens, G. R. and Owen, R. M.: Late Miocene–Early Pliocene manganese redirection in the
987 central Indian Ocean: Expansion of the Intermediate Water oxygen minimum zone,
988 *Paleoceanography*, 9, 169–181, <https://doi.org/10.1029/93pa02699>, 1994.
- 989 Dickens, G. R. and Owen, R. M.: The Latest Miocene–Early Pliocene biogenic bloom: a
990 revised Indian Ocean perspective, *Mar Geol*, 161, 75–91, [https://doi.org/10.1016/s0025-3227\(99\)00057-2](https://doi.org/10.1016/s0025-3227(99)00057-2), 1999.
- 992 Dugdale, R. C.: Chemical oceanography and primary productivity in upwelling regions,
993 *Geoforum*, 3, 47–61, [https://doi.org/10.1016/0016-7185\(72\)90085-1](https://doi.org/10.1016/0016-7185(72)90085-1), 1972.
- 994 Falkowski, P. G.: Evolution of the nitrogen cycle and its influence on the biological
995 sequestration of CO₂ in the ocean, *Nature*, 387, 272–275, <https://doi.org/10.1038/387272a0>,
996 1997.
- 997 Findlater, J.: A major low-level air current near the Indian Ocean during the northern summer,
998 *Q. J. R. Meteorol. Soc.*, 95, 362–380, 1969.

- 999 Flower, B. P. and Kennett, J. P.: The middle Miocene climatic transition: East Antarctic ice
1000 sheet development, deep ocean circulation and global carbon cycling, *Palaeogeogr.*
1001 *Palaeoclimatol. Palaeoecol.*, 108, 537–555, [https://doi.org/10.1016/0031-0182\(94\)90251-8](https://doi.org/10.1016/0031-0182(94)90251-8),
1002 1994.
- 1003 Frigola, A., Prange, M., and Schulz, M.: Boundary conditions for the Middle Miocene
1004 Climate Transition (MMCT v1.0), *Geosci. Model Dev.*, 11, 1607–1626,
1005 <https://doi.org/10.5194/gmd-11-1607-2018>, 2018.
- 1006 Gadgil, S.: The monsoon system: Land–sea breeze or the ITCZ?, *Journal of Earth System*
1007 *Science*, 127, 1–29, <https://doi.org/10.1007/s12040-017-0916-x>, 2018.
- 1008 Garcia, Weathers, K., Paver, C. R., Smolyar, I., Boyer, T. P., Locarnini, R. A., Zweng, M. M.,
1009 Mishonov, A. V., Baranova, O. K., Seidov, D., and Reagan, J. R.: World Ocean Atlas 2018
1010 Volume 3: Dissolved Oxygen, Apparent Oxygen Utilization, and Oxygen Saturation, NOAA
1011 Atlas NESDIS 83, 38 pp., 2018.
- 1012 Garnesson, P., Mangin, A., d’Andon, O. F., Demaria, J., and Bretagnon, M.: The CMEMS
1013 GlobColour chlorophyll a product based on satellite observation: multi-sensor merging and
1014 flagging strategies, *Ocean Sci.*, 15, 819–830, <https://doi.org/10.5194/os-15-819-2019>, 2019.
- 1015 Gaye, B., Böll, A., Segschneider, J., Burdanowitz, N., Emeis, K.-C., Ramaswamy, V.,
1016 Lahajnar, N., Lückge, A., and Rixen, T.: Glacial–interglacial changes and Holocene variations
1017 in Arabian Sea denitrification, *Biogeosciences*, 15, 507–527, [https://doi.org/10.5194/bg-15-](https://doi.org/10.5194/bg-15-507-2018)
1018 [507-2018](https://doi.org/10.5194/bg-15-507-2018), 2018.
- 1019 Gibbs, S., Shackleton, N., and Young, J.: Orbitally forced climate signals in mid-Pliocene
1020 nannofossil assemblages, *Mar. Micropaleontol.*, 51, 39–56,
1021 <https://doi.org/10.1016/j.marmicro.2003.09.002>, 2004a.
- 1022 Gibbs, S. J., Shackleton, N. J., and Young, J. R.: Identification of dissolution patterns in
1023 nannofossil assemblages: A high-resolution comparison of synchronous records from Ceara
1024 Rise, ODP Leg 154, *Paleoceanography*, 19, 1–12, <https://doi.org/10.1029/2003pa000958>,
1025 2004b.
- 1026 Gibbs, S. J., Young, J. R., Bralower, T. J., and Shackleton, N. J.: Nannofossil evolutionary
1027 events in the mid-Pliocene: an assessment of the degree of synchrony in the extinctions of
1028 *Reticulofenestra pseudoumbilicus* and *Sphenolithus abies*, *Palaeogeogr. Palaeoclimatol.*
1029 *Palaeoecol.*, 217, 155–172, <https://doi.org/10.1016/j.palaeo.2004.11.005>, 2005.
- 1030 Gohin, F.: Annual cycles of chlorophyll-*a*, non-algal suspended particulate matter, and
1031 turbidity observed from space and in-situ in coastal waters, *Ocean Sci.*, 7, 705–732,
1032 <https://doi.org/10.5194/os-7-705-2011>, 2011.
- 1033 Gourlan, A. T., Meynadier, L., and Allègre, C. J.: Tectonically driven changes in the Indian
1034 Ocean circulation over the last 25 Ma: Neodymium isotope evidence, *Earth Planet. Sci. Lett.*,
1035 267, 353–364, <https://doi.org/10.1016/j.epsl.2007.11.054>, 2008.
- 1036 Groeneveld, J., Henderiks, J., Renema, W., McHugh, C. M., DeVleeschouwer, D.,
1037 Christensen, B. A., Fulthorpe, C. S., Reuning, L., Gallagher, S. J., Bogus, K., Auer, G.,
1038 Ishiwa, T., and Scientists, E. 356: Australian shelf sediments reveal shifts in Miocene

- 1039 Southern Hemisphere westerlies, *Sci. Adv.*, 3, 1–8, <https://doi.org/10.1126/sciadv.1602567>,
1040 2017.
- 1041 Guieu, C., Azhar, M. A., Aumont, O., Mahowald, N., Levy, M., Ethé, C., and Lachkar, Z.:
1042 Major Impact of Dust Deposition on the Productivity of the Arabian Sea, *Geophys Res Lett*,
1043 46, 6736–6744, <https://doi.org/10.1029/2019gl082770>, 2019.
- 1044 Gupta, A. K. and Thomas, E.: Initiation of Northern Hemisphere glaciation and strengthening
1045 of the northeast Indian monsoon: Ocean Drilling Program Site 758, eastern equatorial Indian
1046 Ocean, *Geology*, 31, 47–50, [https://doi.org/10.1130/0091-
1047 7613\(2003\)031<0047:ionhga>2.0.co;2](https://doi.org/10.1130/0091-7613(2003)031<0047:ionhga>2.0.co;2), 2003.
- 1048 Gupta, A. K., Singh, R. K., Joseph, S., and Thomas, E.: Indian Ocean high-productivity event
1049 (10–8 Ma): Linked to global cooling or to the initiation of the Indian monsoons?, *Geology*,
1050 32, 753–756, <https://doi.org/10.1130/g20662.1>, 2004.
- 1051 Gupta, A. K., Yuvaraja, A., Prakasam, M., Clemens, S. C., and Velu, A.: Evolution of the
1052 South Asian monsoon wind system since the late Middle Miocene, *Palaeogeogr.*
1053 *Palaeoclimatol. Palaeoecol.*, 438, 160–167, <https://doi.org/10.1016/j.palaeo.2015.08.006>,
1054 2015.
- 1055 Hall, R.: Sundaland and Wallacea: Geology, plate tectonics and palaeogeography, edited by:
1056 Gower, D., Johnson, Kenneth, Richardson, James, Rosen, Brian, Ruber, Lukas, and Williams,
1057 S., Cambridge University Press, 32–78, <https://doi.org/10.1017/cbo9780511735882.005>,
1058 2012.
- 1059 Hammer, Ø. and Harper, D. A. T.: *Paleontological Data Analysis*, 1st ed., Blackwell
1060 Publishing Ltd, 2006.
- 1061 Hammer, Ø., Harper, D. A. T., and Ryan, P. D.: PAST: paleontological statistics software
1062 package for education and data analysis, *Palaeontol. Electron.*, 4, 1–9, 2001.
- 1063 Haq, B. U.: Biogeographic history of Miocene calcareous nannoplankton and
1064 paleoceanography of the Atlantic Ocean, *Micropaleontology*, 26, 414–443, 1980.
- 1065 Haq, B. U. and Lohmann, G. P.: Early Cenozoic calcareous nannoplankton biogeography of
1066 the Atlantic Ocean, *Mar. Micropaleontol.*, 1, 119–194, 1976.
- 1067 Harzhauser, M., Kroh, A., Mandic, O., Piller, W. E., Göhlich, U., Reuter, M., and Berning,
1068 B.: Biogeographic responses to geodynamics: A key study all around the Oligo–Miocene
1069 Tethyan Seaway, Special Issue: Phylogenetic Symposium 48th Phylogenetic Symposium on
1070 Historical Biogeography, 246, 241–256, <https://doi.org/10.1016/j.jcz.2007.05.001>, 2007.
- 1071 Holbourn, A., Kuhnt, W., Lyle, M., Schneider, L., Romero, O., and Andersen, N.: Middle
1072 Miocene climate cooling linked to intensification of eastern equatorial Pacific upwelling,
1073 *Geology*, 42, 19–22, <https://doi.org/10.1130/g34890.1>, 2014.
- 1074 Holbourn, A., Kuhnt, W., Kochhann, K. G. D., Andersen, N., and Meier, K. J. S.: Global
1075 perturbation of the carbon cycle at the onset of the Miocene Climatic Optimum, *Geology*, 43,
1076 123–126, <https://doi.org/10.1130/g36317.1>, 2015.

- 1077 Holbourn, A. E., Kuhnt, W., Clemens, S. C., Kochhann, K. G. D., Jöhnck, J., Lübbers, J., and
1078 Andersen, N.: Late Miocene climate cooling and intensification of southeast Asian winter
1079 monsoon, *Nat. Commun.*, 9, 365, <https://doi.org/10.1038/s41467-018-03950-1>, 2018.
- 1080 Honjo, S., Dymond, J., Prell, W., and Ittekkot, V.: Monsoon-controlled export fluxes to the
1081 interior of the Arabian Sea, *Deep Sea Res. Part II Top. Stud. Oceanogr.*, 46, 1859–1902,
1082 [https://doi.org/10.1016/s0967-0645\(99\)00047-8](https://doi.org/10.1016/s0967-0645(99)00047-8), 1999.
- 1083 House, M. A., Rea, D. K., and Janecek, T. R.: Proceedings of the Ocean Drilling Program,
1084 121 Scientific Results, vol. 121, edited by: Weissel, J., Peirce, J., Taylor, E., and Alt, J., 211–
1085 218, <https://doi.org/10.2973/odp.proc.sr.121.133.1991>, 1991.
- 1086 Hu, C., Lee, Z., and Franz, B.: Chlorophyll algorithms for oligotrophic oceans: A novel
1087 approach based on three-band reflectance difference, *J Geophys Res Oceans*, 117,
1088 <https://doi.org/10.1029/2011jc007395>, 2012.
- 1089 Huang, Y., Clemens, S. C., Liu, W., Wang, Y., and Prell, W. L.: Large-scale hydrological
1090 change drove the late Miocene C4 plant expansion in the Himalayan foreland and Arabian
1091 Peninsula, *Geology*, 35, 531–534, 2007a.
- 1092 Huang, Y., Clemens, S. C., Liu, W., Wang, Y., and Prell, W. L.: Large-scale hydrological
1093 change drove the late Miocene C4 plant expansion in the Himalayan foreland and Arabian
1094 Peninsula, *Geology*, 35, 531–534, <https://doi.org/10.1130/g23666a.1>, 2007b.
- 1095 Hutchins, D. A. and Bruland, K. W.: Iron-limited diatom growth and Si:N uptake ratios in a
1096 coastal upwelling regime, *Nature*, 393, 561–564, <https://doi.org/10.1038/31203>, 1998.
- 1097 Imai, R., Farida, M., Sato, T., and Iryu, Y.: Evidence for eutrophication in the northwestern
1098 Pacific and eastern Indian oceans during the Miocene to Pleistocene based on the nannofossil
1099 accumulation rate, Discoaster abundance, and coccolith size distribution of *Reticulofenestra*,
1100 *Mar. Micropaleontol.*, 116, 15–27, <https://doi.org/10.1016/j.marmicro.2015.01.001>, 2015.
- 1101 Imai, R., Sato, T., and Iryu, Y.: Calcareous nannofossil assemblages of the upper Miocene to
1102 Pliocene Shimajiri Group on Okinawa-jima, Ryukyu Islands, southwestern Japan, *J. Asian
1103 Earth Sci.*, 135, 16–24, <https://doi.org/10.1016/j.jseaes.2016.12.011>, 2017.
- 1104 Itou, M., Ono, T., Oba, T., and Noriki, S.: Isotopic composition and morphology of living
1105 *Globorotalia scitula*: a new proxy of sub-intermediate ocean carbonate chemistry?, *Mar.
1106 Micropaleontol.*, 42, 189–210, [https://doi.org/10.1016/s0377-8398\(01\)00015-9](https://doi.org/10.1016/s0377-8398(01)00015-9), 2001.
- 1107 Jatiningrum, R. S. and Sato, T.: Sea-Surface Dynamics Changes in the Subpolar North
1108 Atlantic Ocean (IODP Site U1314) during Late Pliocene Climate Transition Based on
1109 Calcareous Nannofossil Observation, *Open J. Geol.*, 07, 1538–1551,
1110 <https://doi.org/10.4236/ojg.2017.710103>, 2017.
- 1111 Karatsolis, B.-T. and Henderiks, J.: Late Neogene nannofossil assemblages as tracers of ocean
1112 circulation and paleoproductivity over the NW Australian shelf, *Clim Past*, 19, 765–786,
1113 <https://doi.org/10.5194/cp-19-765-2023>, 2023.

- 1114 Keller, G. and Barron, J. A.: Paleooceanographic implications of Miocene deep-sea hiatuses,
1115 Gsa Bulletin, 94, 590–613, [https://doi.org/10.1130/0016-7606\(1983\)94<590:piomdh>2.0.co;2](https://doi.org/10.1130/0016-7606(1983)94<590:piomdh>2.0.co;2), 1983.
- 1117 Kennett, J. P. and Srinivasan, M. S.: Neogene Planktonic Foraminifera: A Phylogenetic Atlas,
1118 Hutchinson Ross; Distributed by worldwide by Van Nostrand Reinhold, Stroudsburg, PA, 265
1119 pp. pp., 1983.
- 1120 Krapivin, V. F. and Varotsos, C. A.: Modelling the CO₂ atmosphere-ocean flux in the
1121 upwelling zones using radiative transfer tools, J. Atmos. Sol.-Terr. Phys., 150, 47–54,
1122 <https://doi.org/10.1016/j.jastp.2016.10.015>, 2016.
- 1123 Kroon, D., Steens, T. N. F., and Troelstra, S. R.: Proceedings of the Ocean Drilling Program,
1124 117 Scientific Results, Proc Ocean Drill Program, 117,
1125 <https://doi.org/10.2973/odp.proc.sr.117.126.1991>, 1991.
- 1126 Kuhnt, W., Holbourn, A., Xu, J., Opdyke, B., Deckker, P. D., Röhl, U., and Mudelsee, M.:
1127 Southern Hemisphere control on Australian monsoon variability during the late deglaciation
1128 and Holocene, Nat. Commun., 6, 5916, <https://doi.org/10.1038/ncomms6916>, 2015.
- 1129 Kunkelova, T., Crocker, A. J., Jewell, A. M., Breeze, P. S., Drake, N. A., Cooper, M. J.,
1130 Milton, J. A., Hennen, M., Shahgedanova, M., Petraglia, M., and Wilson, P. A.: Dust sources
1131 in Westernmost Asia have a different geochemical fingerprint to those in the Sahara,
1132 Quaternary Sci Rev, 294, 107717, <https://doi.org/10.1016/j.quascirev.2022.107717>, 2022.
- 1133 Lahiri, S. P. and Vissa, N. K.: Assessment of Indian Ocean upwelling changes and its
1134 relationship with the Indian monsoon, Global Planet Change, 208, 103729,
1135 <https://doi.org/10.1016/j.gloplacha.2021.103729>, 2022.
- 1136 Laufkötter, C. and Gruber, N.: Will marine productivity wane?, Science, 359, 1103–1104,
1137 <https://doi.org/10.1126/science.aat0795>, 2018.
- 1138 Lee, C., Murray, D. W., Barber, R. T., Buesseler, K. O., Dymond, J., Hedges, J. I., Honjo, S.,
1139 Manganini, S. J., Marra, J., Moser, C., Peterson, M. L., Prell, W. L., and Wakeham, S. G.:
1140 Particulate organic carbon fluxes: compilation of results from the 1995 US JGOFS Arabian
1141 Sea Process Study, Deep Sea Res. Part II Top. Stud. Oceanogr., 45, 2489–2501,
1142 [https://doi.org/10.1016/s0967-0645\(98\)00079-4](https://doi.org/10.1016/s0967-0645(98)00079-4), 1998.
- 1143 LeHouedec, S., Meynadier, L., and Allègre, C. J.: Nd isotope systematics on ODP Sites 756
1144 and 762 sediments reveal major volcanic, oceanic and climatic changes in South Indian Ocean
1145 over the last 35Ma, Earth Planet. Sci. Lett., 327–328, 29–38,
1146 <https://doi.org/10.1016/j.epsl.2012.01.019>, 2012.
- 1147 Lessa, D., Morard, R., Jonkers, L., Venancio, I. M., Reuter, R., Baumeister, A., Albuquerque,
1148 A. L., and Kucera, M.: Distribution of planktonic foraminifera in the subtropical South
1149 Atlantic: depth hierarchy of controlling factors, Biogeosciences, 17, 4313–4342,
1150 <https://doi.org/10.5194/bg-17-4313-2020>, 2020.
- 1151 Ling, A., Eberli, G. P., Swart, P. K., Reolid, J., Stainbank, S., Rüggeberg, A., and Betzler, C.:
1152 Middle Miocene platform drowning in the Maldives associated with monsoon-related

- 1153 intensification of currents, *Palaeogeogr Palaeoclim Palaeoecol*, 567, 110275,
1154 <https://doi.org/10.1016/j.palaeo.2021.110275>, 2021.
- 1155 Litchman, E., Klausmeier, C. A., Miller, J. R., Schofield, O. M., and Falkowski, P. G.: Multi-
1156 nutrient, multi-group model of present and future oceanic phytoplankton communities,
1157 *Biogeosciences*, 3, 585–606, <https://doi.org/10.5194/bg-3-585-2006>, 2006.
- 1158 Lohmann, G. P. and Carlson, J. J.: Oceanographic significance of Pacific Late Miocene
1159 calcareous nannoplankton, *Mar. Micropaleontol.*, 6, 553–579, 1981.
- 1160 Lübbers, J., Kuhnt, W., Holbourn, A. E., Bolton, C. T., Gray, E., Usui, Y., Kochhann, K. G.
1161 D., Beil, S., and Andersen, N.: The middle to late Miocene “Carbonate Crash” in the
1162 equatorial Indian Ocean, *Paleoceanogr. Paleoclimatol.*, 0, 2018PA003482,
1163 <https://doi.org/10.1029/2018pa003482>, 2019.
- 1164 Madhupratap, M., Kumar, S. P., Bhattathiri, P. M. A., Kumar, M. D., Raghukumar, S., Nair,
1165 K. K. C., and Ramaiah, N.: Mechanism of the biological response to winter cooling in the
1166 northeastern Arabian Sea, *Nature*, 384, 549–552, <https://doi.org/10.1038/384549a0>, 1996.
- 1167 Majewski, W.: Water-depth distribution of Miocene planktonic foraminifera from ODP Site
1168 744, southern Indian Ocean, *J Foramin Res*, 33, 144–154, <https://doi.org/10.2113/0330144>,
1169 2003.
- 1170 McCreary, J. P., Yu, Z., Hood, R. R., Vinayachandran, P. N., Furue, R., Ishida, A., and
1171 Richards, K. J.: Dynamics of the Indian-Ocean oxygen minimum zones, *Prog. Oceanogr.*,
1172 112–113, 15–37, <https://doi.org/10.1016/j.pocean.2013.03.002>, 2013.
- 1173 Meisel, S., Struck, U., and Emeis, K.: Nutrient dynamics and oceanographic features in the
1174 central Namibian upwelling region as reflected in $\delta^{15}\text{N}$ -signals of suspended matter and
1175 surface sediments, *Foss Rec*, 14, 153–169, <https://doi.org/10.1002/mmng.201100005>, 2011.
- 1176 Mikaelyan, A. S., Pautova, L. A., Chasovnikov, V. K., Mosharov, S. A., and Silkin, V. A.:
1177 Alternation of diatoms and coccolithophores in the north-eastern Black Sea: a response to
1178 nutrient changes, *Hydrobiologia*, 755, 89–105, <https://doi.org/10.1007/s10750-015-2219-z>,
1179 2015.
- 1180 Miller, K. G., Browning, J. V., Schmelz, W. J., Kopp, R. E., Mountain, G. S., and Wright, J.
1181 D.: Cenozoic sea-level and cryospheric evolution from deep-sea geochemical and continental
1182 margin records, *Sci Adv*, 6, eaaz1346, 2020.
- 1183 Millero, F. J.: The Marine Inorganic Carbon Cycle, *Chem Rev*, 107, 308–341,
1184 <https://doi.org/10.1021/cr0503557>, 2007.
- 1185 Moore, C. M., Mills, M. M., Arrigo, K. R., Berman-Frank, I., Bopp, L., Boyd, P. W.,
1186 Galbraith, E. D., Geider, R. J., Guieu, C., Jaccard, S. L., Jickells, T. D., Roche, J. L., Lenton,
1187 T. M., Mahowald, N. M., Marañón, E., Marinov, I., Moore, J. K., Nakatsuka, T., Oschlies, A.,
1188 Saito, M. A., Thingstad, T. F., Tsuda, A., and Ulloa, O.: Processes and patterns of oceanic
1189 nutrient limitation, 6, 701–710, <https://doi.org/10.1038/ngeo1765>, 2013.
- 1190 Moore, J. K., Fu, W., Primeau, F., Britten, G. L., Lindsay, K., Long, M., Doney, S. C.,
1191 Mahowald, N., Hoffman, F., and Randerson, J. T.: Sustained climate warming drives

- 1192 declining marine biological productivity, *Science*, 359, 1139–1143,
 1193 <https://doi.org/10.1126/science.aao6379>, 2018.
- 1194 Morrison, J. M., Codispoti, L. A., Gaurin, S., Jones, B., Manghnani, V., and Zheng, Z.:
 1195 Seasonal variation of hydrographic and nutrient fields during the US JGOFS Arabian Sea
 1196 Process Study, *Deep Sea Res. Part II Top. Stud. Oceanogr.*, 45, 2053–2101,
 1197 [https://doi.org/10.1016/s0967-0645\(98\)00063-0](https://doi.org/10.1016/s0967-0645(98)00063-0), 1998.
- 1198 Munz, P. M., Siccha, M., Lückge, A., Böll, A., Kucera, M., and Schulz, H.: Decadal-
 1199 resolution record of winter monsoon intensity over the last two millennia from planktic
 1200 foraminiferal assemblages in the northeastern Arabian Sea, *The Holocene*,
 1201 0959683615591357, <https://doi.org/10.1177/0959683615591357>, 2015.
- 1202 Munz, P. M., Steinke, S., Böll, A., Lückge, A., Groeneveld, J., Kucera, M., and Schulz, H.:
 1203 Decadal resolution record of Oman upwelling indicates solar forcing of the Indian summer
 1204 monsoon (9–6 ka), *Clim. Past.*, 13, 491–509, <https://doi.org/10.5194/cp-13-491-2017>, 2017.
- 1205 Naik, D. K., Saraswat, R., Lea, D. W., Kurtarkar, S. R., and Mackensen, A.: Last glacial-
 1206 interglacial productivity and associated changes in the eastern Arabian Sea, *Palaeogeogr*
 1207 *Palaeoclim Palaeoecol*, 483, 147–156, <https://doi.org/10.1016/j.palaeo.2016.07.014>, 2017.
- 1208 Negri, A. and Villa, G.: Calcareous nannofossil biostratigraphy, biochronology and
 1209 paleoecology at the Tortonian/Messinian boundary of the Faneromeni section (Crete),
 1210 *Palaeogeogr. Palaeoclimatol. Palaeoecol.*, 156, 195–209, 2000.
- 1211 Nigrini, C.: Composition and Biostratigraphy of Radiolarian Assemblages from an Area of
 1212 Upwelling (Northwestern Arabian Sea, Leg 117), in: *Proceedings of the Ocean Drilling*
 1213 *Program, 117 Scientific Results*, vol. 117, edited by: Prell, W. J. and Niitsuma, N., 89–126,
 1214 <https://doi.org/10.2973/odp.proc.sr.117.132.1991>, 1991.
- 1215 Nikolaev, S. D., Oskina, N. S., Blyum, N. S., and Bubenshchikova, N. V.: Neogene–
 1216 Quaternary variations of the ‘Pole–Equator’ temperature gradient of the surface oceanic
 1217 waters in the North Atlantic and North Pacific, *Global Planet Change*, 18, 85–111,
 1218 [https://doi.org/10.1016/s0921-8181\(98\)00009-5](https://doi.org/10.1016/s0921-8181(98)00009-5), 1998.
- 1219 Paasche, E.: Roles of nitrogen and phosphorus in coccolith formation in *Emiliania huxleyi*
 1220 (*Prymnesiophyceae*), *Eur J Phycol*, 33, 33–42,
 1221 <https://doi.org/10.1080/09670269810001736513>, 1998.
- 1222 Paerl, H. W.: Why does N-limitation persist in the world’s marine waters?, *Mar. Chem.*, 206,
 1223 1–6, <https://doi.org/10.1016/j.marchem.2018.09.001>, 2018.
- 1224 Pearson, P. N. and Shackleton, N. J.: Neogene multispecies planktonic foraminifer stable
 1225 isotope record, Site 871, Limalok Guyot, in: *Proceedings of the Ocean Drilling Program, 144*
 1226 *Scientific Results*, edited by: Haggerty, J. A., Premoli-Silva, I., Rack, F., and McNutt, M. K.,
 1227 <https://doi.org/10.2973/odp.proc.sr.144.054.1995>, 1995.
- 1228 Pearson, P. N. and Wade, B. S.: Taxonomy and stable isotope paleoecology of well-preserved
 1229 planktonic foraminifera from the uppermost oligocene of Trinidad, *J Foramin Res*, 39, 191–
 1230 217, <https://doi.org/10.2113/gsjfr.39.3.191>, 2009.

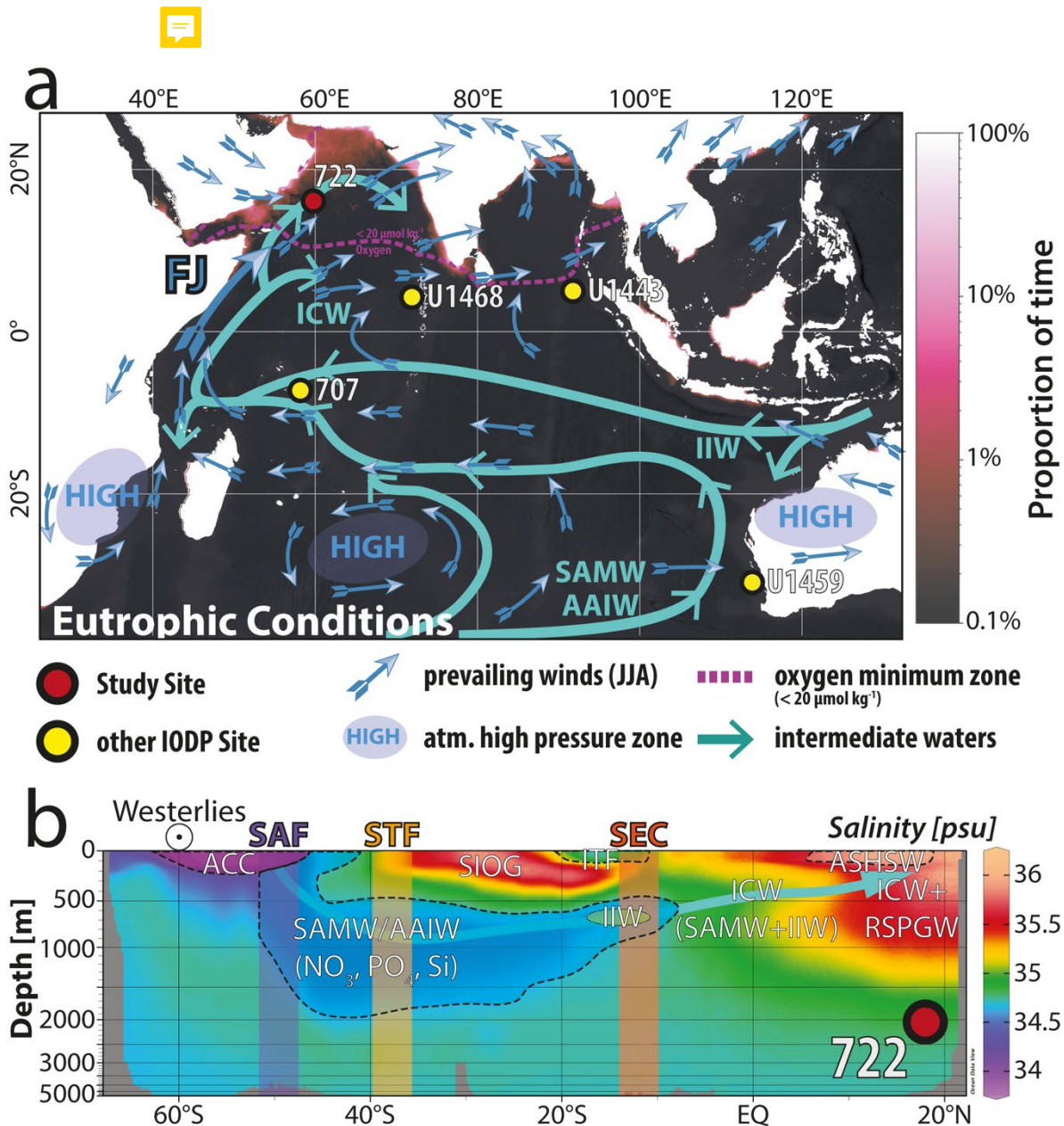
- 1231 Perch-Nielsen, K.: Cenozoic Calcareous Nanofossils, in: *Plankton Stratigraphy*, vol. 1, edited
1232 by: Bolli, H. M., Saunders, J B, and Perch-Nielsen, K., 427–554, 1985.
- 1233 Pound, M. J., Haywood, A. M., Salzmann, U., and Riding, J. B.: Global vegetation dynamics
1234 and latitudinal temperature gradients during the Mid to Late Miocene (15.97–5.33Ma), *Earth-*
1235 *Sci. Rev.*, 112, 1–22, <https://doi.org/10.1016/j.earscirev.2012.02.005>, 2012.
- 1236 Pourmand, A., Marcantonio, F., Bianchi, T. S., Canuel, E. A., and Waterson, E. J.: A 28-ka
1237 history of sea surface temperature, primary productivity and planktonic community variability
1238 in the western Arabian Sea, *Paleoceanography*, 22, n/a-n/a,
1239 <https://doi.org/10.1029/2007pa001502>, 2007.
- 1240 Prell, W. L., Murray, D. W., Clemens, S. C., and Anderson, D. M.: Evolution and Variability
1241 of the Indian Ocean Summer Monsoon: Evidence from the Western Arabian Sea Drilling
1242 Program, edited by: Duncan, R. A., Rea, D. K., Kidd, R. B., Rad, U. von, and Weissel, J. K.,
1243 447–469, <https://doi.org/10.1029/gm070p0447>, 1992.
- 1244 Raven, J. A. and Falkowski, P. G.: Oceanic sinks for atmospheric CO₂, *Plant Cell Environ*,
1245 22, 741–755, <https://doi.org/10.1046/j.1365-3040.1999.00419.x>, 1999.
- 1246 Regenberg, M., Nielsen, S. N., Kuhnt, W., Holbourn, A., Garbe-Schönberg, D., and
1247 Andersen, N.: Morphological, geochemical, and ecological differences of the extant
1248 menardiform planktonic foraminifera *Globorotalia menardii* and *Globorotalia cultrata*, *Mar.*
1249 *Micropaleontol.*, 74, 96–107, <https://doi.org/10.1016/j.marmicro.2010.01.002>, 2010.
- 1250 Reuter, M., Piller, W. E., Harzhauser, M., Kroh, A., and Bassi, D.: Termination of the
1251 Arabian shelf sea: Stacked cyclic sedimentary patterns and timing (Oligocene/Miocene,
1252 Oman), *Sediment Geol*, 212, 12–24, <https://doi.org/10.1016/j.sedgeo.2008.09.001>, 2008.
- 1253 Reuter, M., Piller, W. E., Harzhauser, M., Mandic, O., Berning, B., Rögl, F., Kroh, A., Aubry,
1254 M. P., Wielandt-Schuster, U., and Hamedani, A.: The Oligo-/Miocene Qom Formation (Iran):
1255 evidence for an early Burdigalian restriction of the Tethyan Seaway and closure of its Iranian
1256 gateways, *International Journal of Earth Sciences*, 98, 627-650–650,
1257 <https://doi.org/10.1007/s00531-007-0269-9>, 2009.
- 1258 Reuter, M., Kern, A. K., Harzhauser, M., Kroh, A., and Piller, W. E.: Global warming and
1259 South Indian monsoon rainfall—lessons from the Mid-Miocene, *Gondwana Res.*, 23, 1172–
1260 1177, <https://doi.org/10.1016/j.gr.2012.07.015>, 2013.
- 1261 Reuter, M., Bosellini, F. R., Budd, A. F., Ćorić, S., Piller, W. E., and Harzhauser, M.: High
1262 coral reef connectivity across the Indian Ocean is revealed 6–7 Ma ago by a turbid-water
1263 scleractinian assemblage from Tanzania (Eastern Africa), *Coral Reefs*, 38, 1023–1037,
1264 <https://doi.org/10.1007/s00338-019-01830-8>, 2019.
- 1265 Ridgwell, A. and Zeebe, R. E.: The role of the global carbonate cycle in the regulation and
1266 evolution of the Earth system, *Earth Planet. Sci. Lett.*, 234, 299–315,
1267 <https://doi.org/10.1016/j.epsl.2005.03.006>, 2005.
- 1268 Rixen, T., Goyet, C., and Ittekkot, V.: Diatoms and their influence on the biologically
1269 mediated uptake of atmospheric CO₂ in the Arabian Sea upwelling system, *Biogeosciences*, 3,
1270 1–13, <https://doi.org/10.5194/bg-3-1-2006>, 2006.

- 1271 Rixen, T., Gaye, B., Emeis, K. C., and Ramaswamy, V.: The ballast effect of lithogenic
1272 matter and its influences on the carbon fluxes in the Indian Ocean, *Biogeosciences*, 16, 485–
1273 503, <https://doi.org/10.5194/bg-16-485-2019>, 2019a.
- 1274 Rixen, T., Gaye, B., and Emeis, K.: The Monsoon, Carbon Fluxes, and the Organic Carbon
1275 Pump in the Northern Indian Ocean, *Prog. Oceanogr.*, 175, 24–39,
1276 <https://doi.org/10.1016/j.pocean.2019.03.001>, 2019b.
- 1277 Rodriguez, M., Chamot-Rooke, N., Huchon, P., Fournier, M., and Delescluse, M.: The Owen
1278 Ridge uplift in the Arabian Sea: Implications for the sedimentary record of Indian monsoon in
1279 Late Miocene, *Earth Planet. Sci. Lett.*, 394, 1–12, <https://doi.org/10.1016/j.epsl.2014.03.011>,
1280 2014.
- 1281 Rodriguez, M., Bourget, J., Chamot-Rooke, N., Huchon, P., Fournier, M., Delescluse, M., and
1282 Zaragosi, S.: The Sawqirah contourite drift system in the Arabian Sea (NW Indian Ocean): A
1283 case study of interactions between margin reactivation and contouritic processes, *Mar Geol.*,
1284 381, 1–16, <https://doi.org/10.1016/j.margeo.2016.08.004>, 2016.
- 1285 Rögl, F.: Mediterranean and Paratethys. Facts and hypotheses of an Oligocene to Miocene
1286 paleogeography (short overview), *Geologica Carpathica*, 50, 339–349, 1999.
- 1287 Samtleben, C.: Die Evolution der Coccolithophoriden-Gattung *Gephyrocapsa* nach Befunden
1288 im Atlantik, *PalZ*, 54, 91–127–127, <https://doi.org/10.1007/bf02985885>, 1980.
- 1289 Sarmiento, J. L. and Gruber, N.: Ocean Biogeochemical Dynamics, 359–391,
1290 <https://doi.org/10.2307/j.ctt3fgxqx.13>, 2013.
- 1291 Sarmiento, J. L., Gruber, N., Brzezinski, M. A., and Dunne, J. P.: High-latitude controls of
1292 thermocline nutrients and low latitude biological productivity, *Nature*, 427, 56–60,
1293 <https://doi.org/10.1038/nature02127>, 2004.
- 1294 Sarr, A.-C., Donnadiou, Y., Bolton, C. T., Ladant, J.-B., Licht, A., Fluteau, F., Laugié, M.,
1295 Tardif, D., and Dupont-Nivet, G.: Neogene South Asian monsoon rainfall and wind histories
1296 diverged due to topographic effects, *Nat Geosci*, 15, 314–319, [https://doi.org/10.1038/s41561-
1297 022-00919-0](https://doi.org/10.1038/s41561-022-00919-0), 2022.
- 1298 Schiebel, R., Zeltner, A., Treppke, U. F., Waniek, J. J., Bollmann, J., Rixen, T., and
1299 Hemleben, C.: Distribution of diatoms, coccolithophores and planktic foraminifers along a
1300 trophic gradient during SW monsoon in the Arabian Sea, *Mar. Micropaleontol.*, 51, 345–371,
1301 <https://doi.org/10.1016/j.marmicro.2004.02.001>, 2004.
- 1302 Schlitzer, R.: Ocean Data View, 2021.
- 1303 Schott, F. A. and McCreary, J. P.: The monsoon circulation of the Indian Ocean, *Prog.*
1304 *Oceanogr.*, 51, 1–123, 2001.
- 1305 Schott, F. A., Xie, S.-P., and Jr., J. P. M.: Indian Ocean circulation and climate variability,
1306 *Reviews of Geophysics*, 47, 3295, <https://doi.org/10.1029/2007rg000245>, 2009.

- 1307 Schubert, C. J., Villanueva, J., Calvert, S. E., Cowie, G. L., Rad, U. von, Schulz, H., Berner,
1308 U., and Erlenkeuser, H.: Stable phytoplankton community structure in the Arabian Sea over
1309 the past 200,000 years, *Nature*, 394, 563–566, <https://doi.org/10.1038/29047>, 1998.
- 1310 Schueth, J. D. and Bralower, T. J.: The relationship between environmental change and the
1311 extinction of the nannoplankton Discoaster in the early Pleistocene, *Paleoceanography*, 30,
1312 863–876, <https://doi.org/10.1002/2015pa002803>, 2015.
- 1313 Sexton, P. F. and Norris, R. D.: High latitude regulation of low latitude thermocline
1314 ventilation and planktic foraminifer populations across glacial–interglacial cycles, *Earth*
1315 *Planet. Sci. Lett.*, 311, 69–81, <https://doi.org/10.1016/j.epsl.2011.08.044>, 2011.
- 1316 Shimmield, G. B.: Can sediment geochemistry record changes in coastal upwelling
1317 palaeoproductivity? Evidence from northwest Africa and the Arabian Sea, *Geological Soc*
1318 *Lond Special Publ*, 64, 29–46, <https://doi.org/10.1144/gsl.sp.1992.064.01.03>, 1992.
- 1319 Shipboard-Scientific-Party: Site 722, vol. 117,
1320 <https://doi.org/10.2973/odp.proc.ir.117.107.1989>, 1989.
- 1321 Sigman, D. M. and Fripiat, F.: Nitrogen Isotopes in the Ocean, in: *Encyclopedia of Ocean*
1322 *Sciences (Third Edition)*, edited by: Cochran, J. K., Bokuniewicz, H. J., and Yager, P. L.,
1323 263–278, <https://doi.org/10.1016/b978-0-12-409548-9.11605-7>, 2019.
- 1324 Smart, C. W., Thomas, E., and Ramsay, A. T. S.: Middle–late Miocene benthic foraminifera
1325 in a western equatorial Indian Ocean depth transect: Paleoceanographic implications,
1326 *Palaeogeogr. Palaeoclimatol. Palaeoecol.*, 247, 402–420,
1327 <https://doi.org/10.1016/j.palaeo.2006.11.003>, 2007.
- 1328 Sokal, R. R. and Rohlf, F. J.: *Biometry*, 3rd ed., W. H. Freeman and Company, 1995.
- 1329 Sosdian, S. M. and Lear, C. H.: Initiation of the Western Pacific Warm Pool at the Middle
1330 Miocene Climate Transition?, *Paleoceanogr. Paleoclimatol.*,
1331 <https://doi.org/10.1029/2020pa003920>, 2020.
- 1332 Spezzaferri, S.: Planktonic foraminiferal paleoclimatic implications across the Oligocene-
1333 Miocene transition in the oceanic record (Atlantic, Indian and South Pacific), *Palaeogeogr*
1334 *Palaeoclim Palaeoecol*, 114, 43–74, [https://doi.org/10.1016/0031-0182\(95\)00076-x](https://doi.org/10.1016/0031-0182(95)00076-x), 1995.
- 1335 Stramma, L., Johnson, G. C., Sprintall, J., and Mohrholz, V.: Expanding Oxygen-Minimum
1336 Zones in the Tropical Oceans, *Science*, 320, 655–658,
1337 <https://doi.org/10.1126/science.1153847>, 2008.
- 1338 Suess, E.: Particulate organic carbon flux in the oceans—surface productivity and oxygen
1339 utilization, *Nature*, 288, 260–263, <https://doi.org/10.1038/288260a0>, 1980.
- 1340 Taucher, J., Bach, L. T., Prowe, A. E. F., Boxhammer, T., Kvale, K., and Riebesell, U.:
1341 Enhanced silica export in a future ocean triggers global diatom decline, *Nature*, 605, 696–700,
1342 <https://doi.org/10.1038/s41586-022-04687-0>, 2022.
- 1343 ThiDieuVu, H. and Sohrin, Y.: Diverse stoichiometry of dissolved trace metals in the Indian
1344 Ocean, *Sci. Rep.*, 3, 1745, <https://doi.org/10.1038/srep01745>, 2013.

- 1345 Toggweiler, J. R., Druffel, E. R. M., Key, R. M., and Galbraith, E. D.: Upwelling in the
 1346 Ocean Basins North of the ACC: 1. On the Upwelling Exposed by the Surface Distribution of
 1347 $\Delta^{14}\text{C}$, *J. Geophys. Res.: Oceans*, 124, 2591–2608, <https://doi.org/10.1029/2018jc014794>,
 1348 2019a.
- 1349 Toggweiler, J. R., Druffel, E. R. M., Key, R. M., and Galbraith, E. D.: Upwelling in the
 1350 Ocean Basins North of the ACC: 1. On the Upwelling Exposed by the Surface Distribution of
 1351 $\Delta^{14}\text{C}$, *J. Geophys. Res.: Oceans*, 124, 2591–2608, <https://doi.org/10.1029/2018jc014794>,
 1352 2019b.
- 1353 Tomczak, M. and Godfrey, J. S.: *Hydrology of the Indian Ocean*, edited by: Tomczak, M. and
 1354 Godfrey, J. S., Daya Publishing House, 199–214, 2003.
- 1355 Tripathi, S., Tiwari, M., Lee, J., Khim, B.-K., Pandey, D. K., Clift, P. D., Kulhanek, D. K.,
 1356 Andò, S., Bendle, J. A. P., Aharonovich, S., Griffith, E. M., Gurusurthy, G. P., Hahn, A.,
 1357 Iwai, M., Kumar, A., Kumar, A. G., Liddy, H. M., Lu, H., Lyle, M. W., Mishra, R.,
 1358 Radhakrishna, T., Routledge, C. M., Saraswat, R., Saxena, R., Scardia, G., Sharma, G. K.,
 1359 Singh, A. D., Steinke, S., Suzuki, K., Tauxe, L., Xu, Z., and Yu, Z.: First evidence of
 1360 denitrification vis-à-vis monsoon in the Arabian Sea since Late Miocene, *Sci. Rep.*, 7, 43056,
 1361 <https://doi.org/10.1038/srep43056>, 2017.
- 1362 Tudhope, A. W., Lea, D. W., Shimmield, G. B., Chilcott, C. P., and Head, S.: Monsoon
 1363 Climate and Arabian Sea Coastal Upwelling Recorded in Massive Corals from Southern
 1364 Oman, *Palaios*, 11, 347, <https://doi.org/10.2307/3515245>, 1996.
- 1365 Ustick, L. J., Larkin, A. A., Garcia, C. A., Garcia, N. S., Brock, M. L., Lee, J. A., Wiseman,
 1366 N. A., Moore, J. K., and Martiny, A. C.: Metagenomic analysis reveals global-scale patterns
 1367 of ocean nutrient limitation, *Science*, 372, 287–291, <https://doi.org/10.1126/science.abe6301>,
 1368 2021.
- 1369 Villa, G., Fioroni, C., Pea, L., Bohaty, S., and Persico, D.: Middle Eocene–late Oligocene
 1370 climate variability: Calcareous nannofossil response at Kerguelen Plateau, Site 748, Mar.
 1371 *Micropaleontol.*, 69, 173–192, <https://doi.org/10.1016/j.marmicro.2008.07.006>, 2008.
- 1372 Volk, T. and Hoffert, M. I.: Ocean Carbon Pumps: Analysis of Relative Strengths and
 1373 Efficiencies in Ocean-Driven Atmospheric CO₂ Changes, in: *The Carbon Cycle and*
 1374 *Atmospheric CO₂: Natural Variations Archean to Present*, vol. 32, edited by: Sundquist, E. T.
 1375 and Broecker, W. S., 99–110, <https://doi.org/10.1029/gm032p0099>, 1985.
- 1376 Wade, B. S. and Bown, P. R.: Calcareous nannofossils in extreme environments: The
 1377 Messinian Salinity Crisis, Polemi Basin, Cyprus, *Palaeogeogr. Palaeoclimatol. Palaeoecol.*,
 1378 233, 271–286, <https://doi.org/10.1016/j.palaeo.2005.10.007>, 2006.
- 1379 Wang, D., Gouhier, T. C., Menge, B. A., and Ganguly, A. R.: Intensification and spatial
 1380 homogenization of coastal upwelling under climate change, *Nature*, 518, 390–394,
 1381 <https://doi.org/10.1038/nature14235>, 2015.
- 1382 Wei, W. and Wise, S. W.: Biogeographic gradients of middle Eocene–Oligocene calcareous
 1383 nannoplankton in the South Atlantic Ocean, *Palaeogeogr. Palaeoclimatol. Palaeoecol.*, 79, 29–
 1384 61, 1990.

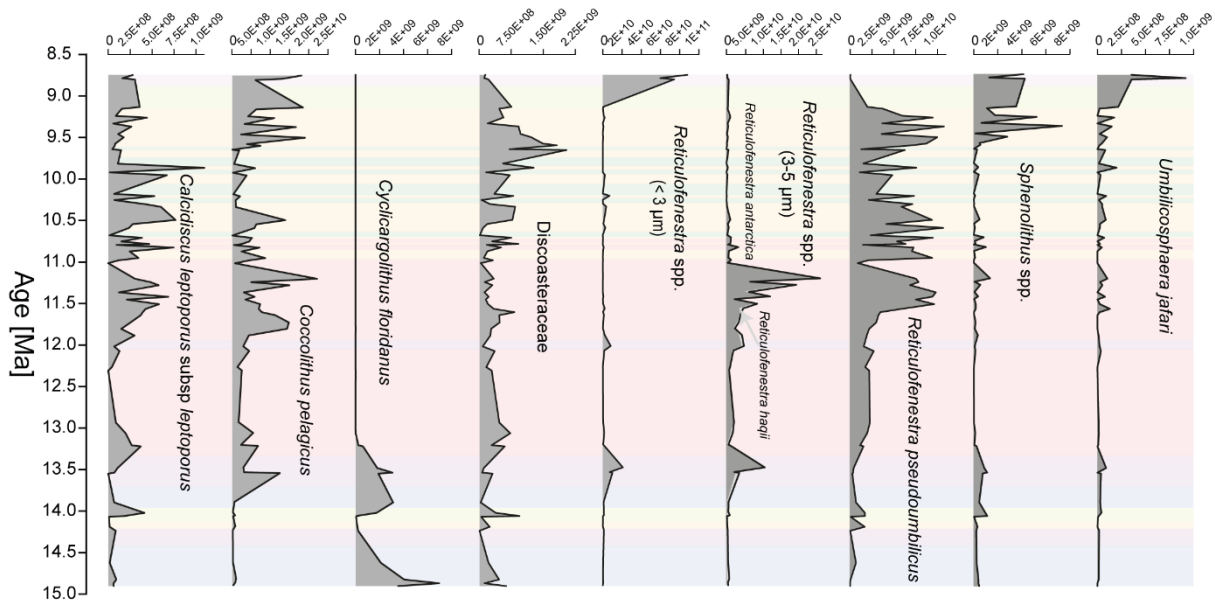
- 1385 Westerhold, T., Marwan, N., Drury, A. J., Liebrand, D., Agnini, C., Anagnostou, E., Barnet, J.
 1386 S. K., Bohaty, S. M., Vleeschouwer, D. D., Florindo, F., Frederichs, T., Hodell, D. A.,
 1387 Holbourn, A. E., Kroon, D., Lauretano, V., Littler, K., Lourens, L. J., Lyle, M., Pälike, H.,
 1388 Röhl, U., Tian, J., Wilkens, R. H., Wilson, P. A., and Zachos, J. C.: An astronomically dated
 1389 record of Earth's climate and its predictability over the last 66 million years, *Science*, 369,
 1390 1383–1387, <https://doi.org/10.1126/science.aba6853>, 2020.
- 1391 Woodruff, F. and Savin, S. M.: Miocene deepwater oceanography, *Paleoceanography*, 4, 87–
 1392 140, <https://doi.org/10.1029/pa004i001p00087>, 1989.
- 1393 Woodward, E. M. S., Rees, A. P., and Stephens, J. A.: The influence of the south-west
 1394 monsoon upon the nutrient biogeochemistry of the Arabian Sea, *Deep Sea Res. Part II Top.*
 1395 *Stud. Oceanogr.*, 46, 571–591, [https://doi.org/10.1016/s0967-0645\(98\)00118-0](https://doi.org/10.1016/s0967-0645(98)00118-0), 1999.
- 1396 Yang, X., Groeneveld, J., Jian, Z., Steinke, S., and Giosan, L.: Middle Miocene Intensification
 1397 of South Asian Monsoonal Rainfall, *Paleoceanogr. Paleoclimatol.*, 35,
 1398 <https://doi.org/10.1029/2020pa003853>, 2020.
- 1399 Yao, Z., Shi, X., Guo, Z., Li, X., Nath, B. N., Betzler, C., Zhang, H., Lindhorst, S., and
 1400 Miriyala, P.: Weakening of the South Asian summer monsoon linked to interhemispheric ice-
 1401 sheet growth since 12 Ma, *Nat. Commun.*, 14, 829, [https://doi.org/10.1038/s41467-023-](https://doi.org/10.1038/s41467-023-36537-6)
 1402 [36537-6](https://doi.org/10.1038/s41467-023-36537-6), 2023.
- 1403 You, Y.: Seasonal variations of thermocline circulation and ventilation in the Indian Ocean, *J.*
 1404 *Geophys. Res.: Oceans*, 102, 10391–10422, <https://doi.org/10.1029/96jc03600>, 1997.
- 1405 You, Y.: Intermediate water circulation and ventilation of the Indian Ocean derived from
 1406 water-mass contributions, 1 January 1998.
- 1407 You, Y. and Tomczak, M.: Thermocline circulation and ventilation in the Indian Ocean
 1408 derived from water mass analysis, *Deep Sea Res. Part : Oceanogr. Res. Pap.*, 40, 13–56,
 1409 [https://doi.org/10.1016/0967-0637\(93\)90052-5](https://doi.org/10.1016/0967-0637(93)90052-5), 1993.
- 1410 Young, J.: Size variation of Neogene *Reticulofenestra* coccoliths from Indian Ocean DSDP
 1411 Cores, *J Micropalaeontol*, 9, 71–85, <https://doi.org/10.1144/jm.9.1.71>, 1990.
- 1412 Young, J. R.: Neogene, in: *Calcareous Nannofossil Biostratigraphy*, edited by: Bown, P. R.,
 1413 225–265, 1998.
- 1414 Nannotax 3: <http://www.mikrotax.org/Nannotax3/>, last access: 24 July 2023.
- 1415 Zhang, Z., Ramstein, G., Schuster, M., Li, C., Contoux, C., and Yan, Q.: Aridification of the
 1416 Sahara desert caused by Tethys Sea shrinkage during the Late Miocene, *Nature*, 513, 401–
 1417 404, <https://doi.org/10.1038/nature13705>, 2014.
- 1418 Zhuang, G., Pagani, M., and Zhang, Y. G.: Monsoonal upwelling in the western Arabian Sea
 1419 since the middle Miocene, *Geology*, 45, 655–658, <https://doi.org/10.1130/g39013.1>, 2017.
- 1420 Zweng, M. M., Reagan, J. R., Seidov, D., Boyer, T. P., Locarnini, M. M., Garcia, H. E.,
 1421 Mishonov, A. V., Baranova, O. K., Weathers, K. W., Paver, C. R., and Smolyar, I.: *World*
 1422 *ocean atlas 2018, Volume 2: Salinity*, edited by: Mishonov, A., 50 pp., 2019.



1424

1425 **Figure 1:** a) Location map showing the study site ODP Site 722 and IODP Site U1468 and the prevalent summertime
 1426 wind patterns following Bialik et al. (2020a). Generalized flow flow-paths of dominant intermediate waters of the **indian**
 1427 Ocean follow You (1998) and Böning (2009), The present-day extent of the oxygen minimum zone is shown as a pink
 1428 dashed line denoting oxygen concentrations <math>< 20 \mu\text{mol kg}^{-1}</math> at a water depth of 200 m (McCreary et al., 2013; Garcia et
 1429 al., 2018). Eutrophication (magenta shading) data was provided by the E.U. Copernicus Marine Service Information
 1430 using the Global Ocean Colour (Copernicus-GlobColour), Bio-Geo-Chemical, L4 (monthly and interpolated) from
 1431 Satellite Observations (1997-ongoing); <https://doi.org/10.48670/moi-00281>. Shading represents gap-filled daily
 1432 Chlorophyll-a product of Copernicus GLOBColour L4 (Gohin, 2011; Hu et al., 2012; Garnesson et al., 2019) and
 1433 indicates the proportion of time spent in eutrophic conditions in the region, based on the proportion of days (1998-2022)
 1434 where Chlorophyll-a concentration exceeded a threshold of 7.3 mg m⁻³ (derived from Carlson, 1977). The python code
 1435 used to generate the base map is available in the supplementary material; b) **Salinity** profile generated based on the
 1436 world Ocean Atlas 2018 salinity data (Zweng et al., 2019) through the Indian Ocean from 65°S to 20°N. The plot was
 1437 generated using Ocean Data View (Schlitzer, 2021). Water masses are differentiated based on their salinity signature
 1438 outlined with dashed lines and labeled. Furthermore major frontal systems and currents are also indicated.
 1439 Abbreviations: **Antarctic Intermediate Water (AAIW)**, **Antarctic Circumpolar Current (ACC)**, **Arabian Sea High**
 1440 **Salinity Water (ASHSW)**, **Indian Central Water (ICW)**, **Indonesian Intermediate Water (IIW)**, **Red Sea/Persian Gulf**
 1441 **Water (RSPGW)**, **sub-Antarctic Mode Water (SAMW)**, **Southern Indian Ocean Gyre (SIOG)**,

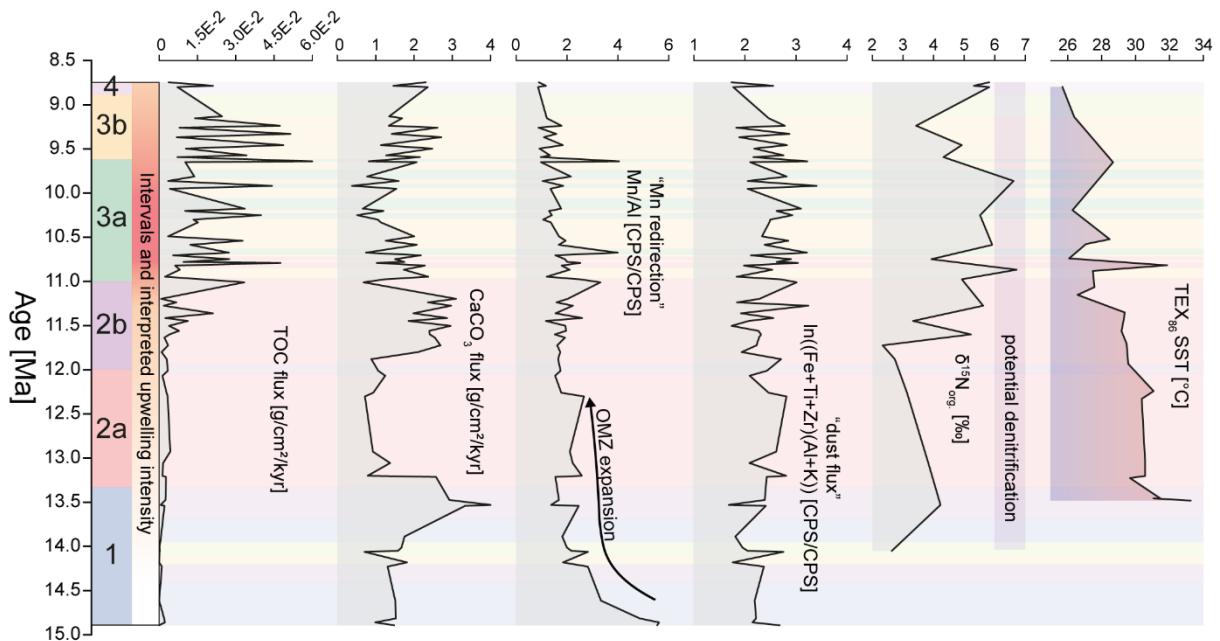
1442



1443

1444 **Figure 2: Abundance data of key nanofossil taxa presented as numbers per gram of carbonate over the study interval**
 1445 **following the methods of Bordiga et al. (2015). The used age model is based on Bialik et al. (2020a). Medium-sized**
 1446 **reticulofenestrids are separated into morphotypes with an open central area (Reticulofenestra haqii) and a closed**
 1447 **central area (R antarctica). Discoasteraceae include the genera Discoaster and Catinaster. Color coding represents the**
 1448 **cluster assignment based on the nanofossil assemblage shown in fig. 4a.**

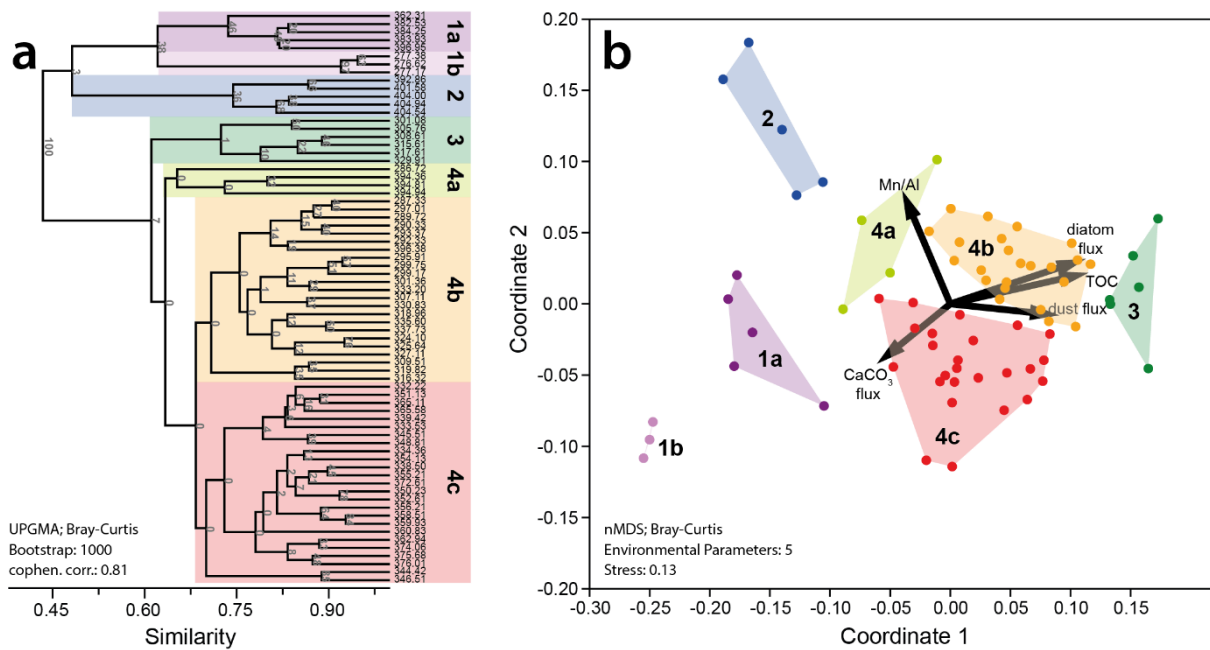
1449



1450

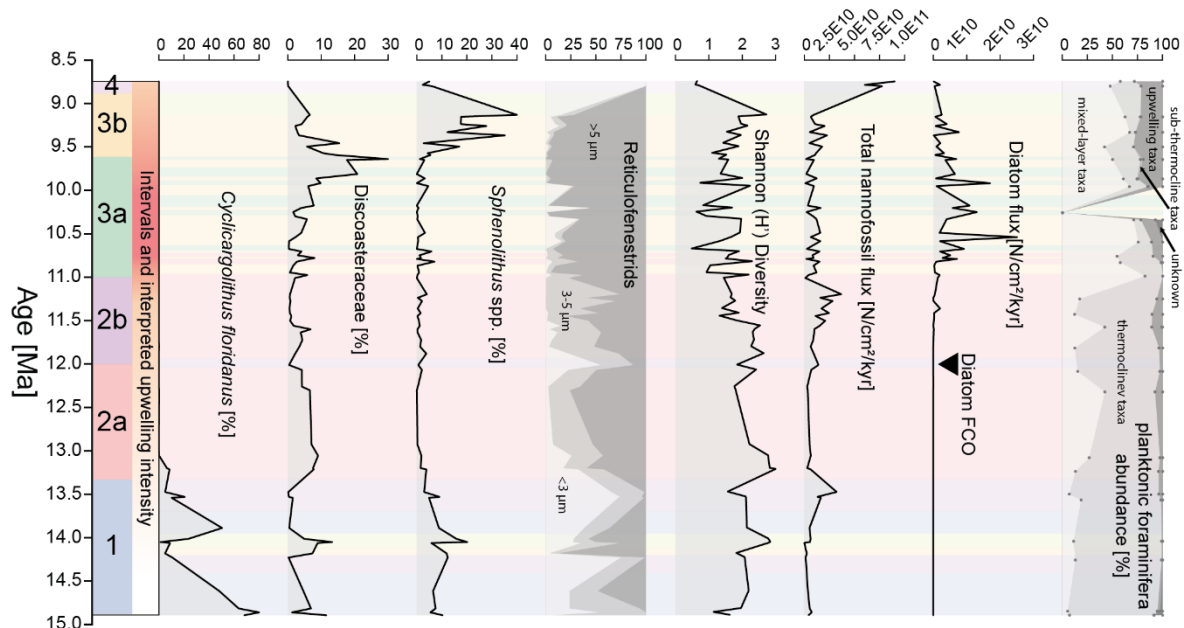
1451 **Figure 3: Geochemical data initially published by Bialik et al. (2020a) as well as TEX_{86}^H based SST data of Zhuang et al.**
 1452 **(2017). Data is shown in conjunction with the cluster analysis results based on the nanofossil assemblages, as shown in**
 1453 **figure 4a. Total organic carbon (TOC in wt.%) is based on bulk sediment measurements. The Mn/Al ratio and the**
 1454 **shown dust flux proxy, are based on benchtop XRF counts. Dust flux is calculated as $\ln((Zr+Ti+Fe)/(Al+K))$ based on**
 1455 **Kuhnt et al. (2015), with higher values indicating higher deposition of dust-born minerals at Site 722. Nitrogen isotopic**
 1456 **data indicate increasing denitrification of sinking organic matter with higher values. On the left of the figure we also**
 1457 **show intervals 1 – 4 and their respective sub-intervals a/b and the resulting interpreted upwelling intensity. All data is**
 1458 **underpinned by the assigned clusters as defined in Figure 4.**

1459



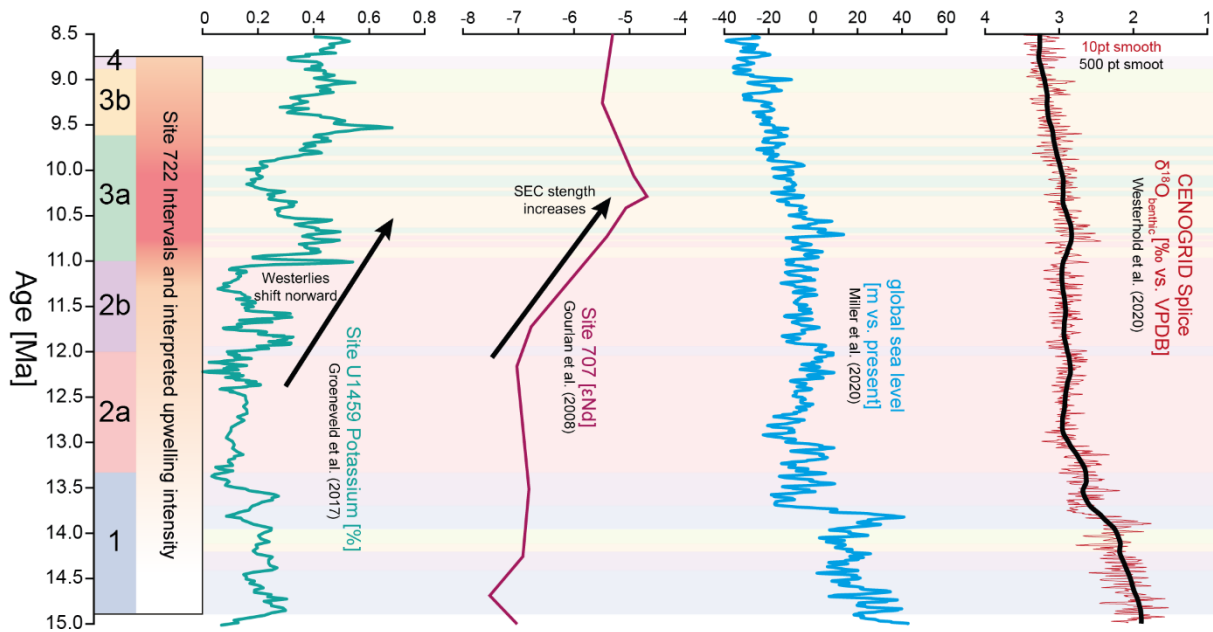
1460
1461
1462
1463
1464
1465
1466
1467
1468

Figure 4: Cluster analysis (a) and nMDS (b) based on the datasets shown in Figs. 2 and 3. The geochemical data serves as paleoenvironmental proxies for high productivity (total organic carbon and siliceous fragments), high wind intensity (dust flux), water column oxygenation (Mn/Al), and high carbonate accumulation (CaCO₃ flux). Note the high correspondence of clusters 3 and, to some degree, 4b diatom accumulation, dust flux, and high TOC content. They indicate that these clusters likely correspond to nannofossil assemblages thriving during intense upwelling. Conversely, lower productivity and, thus, higher water column oxygenation are marked by a correspondence of clusters 2 and 4a with higher Mn/Al values, denoting a less intense oxygen minimum zone.



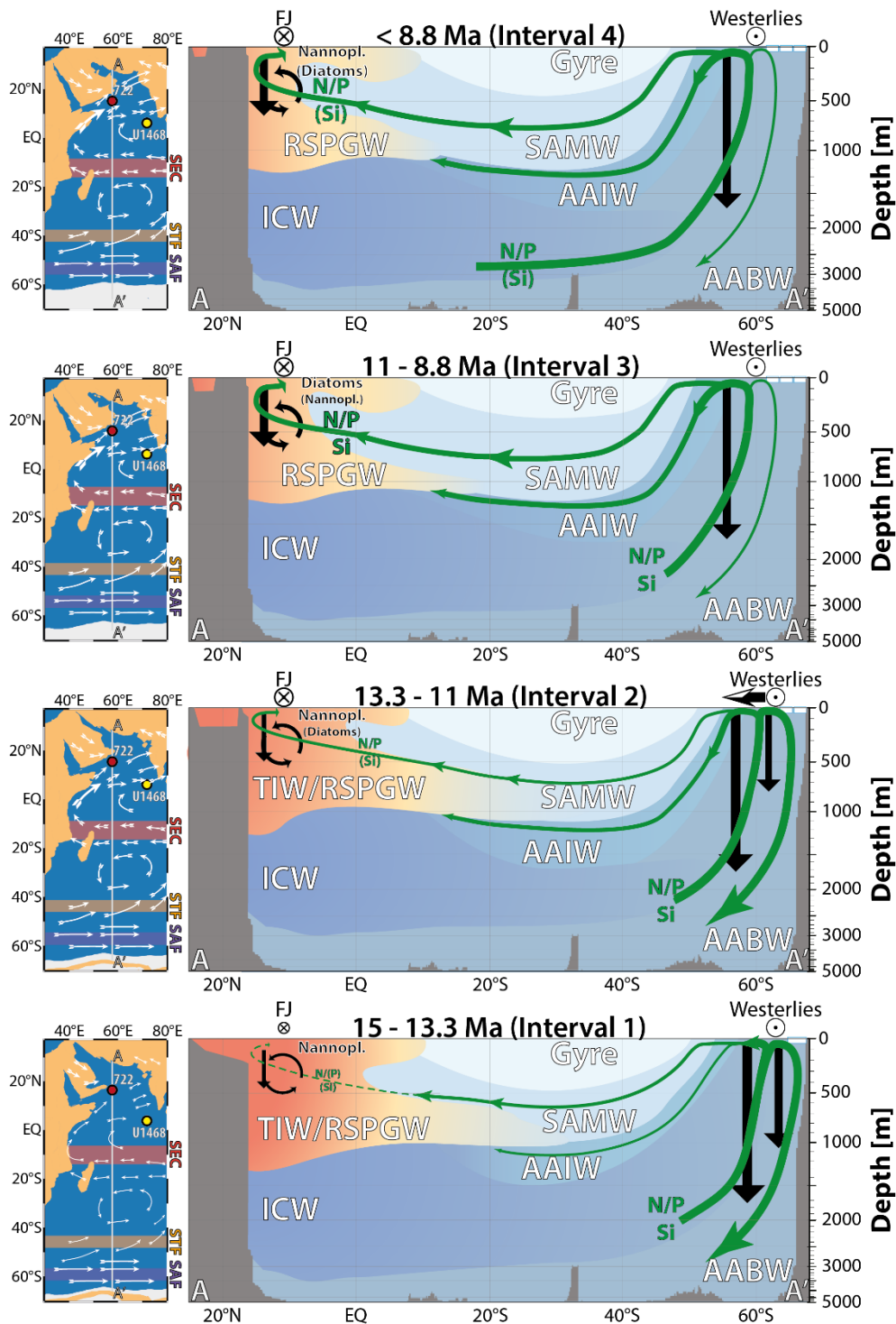
1469
1470
1471
1472
1473
1474
1475
1476
1477
1478
1479
1480

Figure 5: Summary of relevant nannofossil taxa (*C. floridanus*, the sum of all Discoasteraceae, *Sphenolithus* spp., as well as all 3 selected size ranges of *Reticulofenestra* spp.) shown as % abundance of the whole assemblage. Reticulofenestrads are combined into a single abundance graph showing the internal variability of the three defined size ranges of the genus *Reticulofenestra*. The Shannon (H') diversity is offered as an overall indicator of nanoplankton diversity throughout the study interval. The total abundance of nannofossils fluxes in N/cm²/kyr illustrates the stark increase in nannofossil accumulation in interval 4, denoting the noted bloom in small reticulofenestrads after 8.8 Ma. Next, the nannofossil abundances are contrasted with diatom fluxes. The nannofossil assemblage variability is further shown with classical upwelling indicators based on planktonic foraminifera, which shows an overall constant abundance of upwelling indicative taxa (e.g., *G. bulloides*) between Interval 3a and 4, despite the dynamic changes in the phytoplankton data. On the left of the figure we also show intervals 1 – 4 and their respective sub-intervals a/b and the resulting interpreted upwelling intensity. All data is underpinned by the assigned clusters as defined in Figure 4.



1481
 1482 **Figure 6: Compilation of Indian Ocean and Global Data during the Study interval. Proposed plankton community**
 1483 **intervals as well as nannofossil assemblages at Site 772 are presented next to the abundance of natural gamma radiation**
 1484 **derived potassium content at Site U1459 (Groeneveld et al., 2017), interpreted to relate to precipitation changes in**
 1485 **western Australia as a consequence of the northward shifting southern hemisphere westerlies. The εNd data of Gourlan**
 1486 **et al. (2008), showing an increase in εNd signatures derived from Indonesia Indicating an increase in SEC strength, due**
 1487 **to a global increase in global ocean and atmospheric circulation (e.g., Betzler and Eberli, 2019). The global sea level**
 1488 **reconstruction of Miller et al. (2020) showing stable sea levels after the MMCT until at least 11 Ma. The global stable**
 1489 **CENOGRID stable oxygen isotope stack for the study interval, showing stable deep water conditions until 11 Ma**
 1490 **(Westerhold et al., 2020). On the left of the figure we also show intervals 1 – 4 and their respective sub-intervals a/b and**
 1491 **the resulting interpreted upwelling intensity. All data is underpinned by the assigned clusters as defined in Figure 4.**

1492



1493

1494 Figure 7: Envisioned progression of upwelling along the Oman Margin based on paleogeography of Cao et al. (2017),
 1495 adapted with regional information (Rögl, 1999; Bialik et al., 2019; Reuter et al., 2009, 2008), combined with
 1496 hypothesized changing intermediate water-based nutrient supply throughout the study interval (c. 15 – 8 Ma). The
 1497 figure also shows the hypothesized change in water masses over the study interval. Orange shading represents local
 1498 water masses forming in the northern Indian Ocean migrating southward. While intermediate waters able to
 1499 progressively migrate further in the the Arabian Sea where ~~the~~ begin to dominate upwelling by c. 11 Ma. Shading of
 1500 the water masses represents their progressive intermixing with each other. Water masses shown are the Tethyan
 1501 Intermediate Water (TIW), the Red Sea and Persian Gulf Intermediate Waters (RSPGW), Indian Central Water
 1502 (ICW), southern Indian Ocean gyre waters (Gyre), sub-Antarctic mode water (SAMW), and the Antarctic intermediate
 1503 water (AAIW) and Antarctic bottom water (AABW). In addition, note the corresponding change in nutrient (N, P,
 1504 and Si) transport – **visualized** by green arrows - following the proposed northward migration of the southern hemisphere
 1505 westerlies due to sea ice expansion after 12 Ma (Groeneveld et al., 2017). Hypothesized changes in nutrient transport
 1506 are based on model studies, which predict reduced low-latitude productivity during warmer climates (Laufkötter and

1507 Gruber, 2018; Moore et al., 2018). Black arrows indicate the changes in the fluxes and hypothesized recycling of organic
 1508 matter within the WAS upwelling zone.

1509 **Table 1: Ecological interpretation of the defined nannofossil taphogroups based on the ecological parameters of the**
 1510 **defining nannofossil taxa.**

<i>Tapho- group</i>	<i>Defining Taxa</i>	<i>Ecology</i>	<i>References</i>	<i>Environmental Parameters</i>
<i>TG1a</i>	<i>Reticulofenestra minuta</i> dominant	Dominated by r-selected opportunistic nannofossil taxa. Commonly interpreted as nutrient elevation in the photic zone.	(Haq, 1980; Wade and Bown, 2006; Auer et al., 2015)	Associated with high calcium carbonate accumulation
<i>TG1b</i>	Small and medium reticulofenestrids together with <i>Cyclicargolithus floridanus</i>	Warm to temperate waters, with increased nutrient conditions.	(Wei and Wise, 1990; Wade and Bown, 2006; Auer et al., 2015)	Associated with high calcium carbonate accumulation
<i>TG2</i>	<i>Cyclicargolithus floridanus</i> and common medium reticulofenestrids	Warm to temperate waters, with moderate nutrient conditions.	(Wei and Wise, 1990; Wade and Bown, 2006; Auer et al., 2015)	Associated with high Mn/Al ratios (= weak OMZ) and elevated carbonate content
<i>TG3</i>	Large reticulofenestrids dominant with common Discoasterids	Elevated nutrient conditions with deep nutricline and possible (seasonal) stratification	(Lohmann and Carlson, 1981; Backman et al., 2013; Imai et al., 2015, 2017)	Associated with biogenic silica, TOC, dust flux and lowered Mn/Al ratios (=stronger OMZ)
<i>TG4a</i>	Variable small, medium and large reticulofenestrids with common <i>Sphenolithus</i> spp. and discoasterids	Elevated nutrient conditions with high seasonal variability and intermittent stratification, possible indication of increased environmental stress.	(Castradori, 1998; Blanc-Valleron et al., 2002; Gibbs et al., 2004b; Wade and Bown, 2006; Villa et al., 2008; Beltran et al., 2014; Imai et al., 2015; Schueth and Bralower, 2015)	Weakly associated with carbonate accumulation and higher Mn/Al ratios (= weak OMZ)
<i>TG4b</i>	Large reticulofenestrids dominant	High nutrient conditions, likely open marine and potentially stratified.	(Auer et al., 2014, 2015; Beltran et al., 2014; Imai et al., 2017, 2015)	Weakly associated with biogenic silica flux, TOC and reduced Mn/Al ratios (= increasing OMZ)
<i>TG4c</i>	Medium and large reticulofenestrids dominant	High nutrient levels, likely upwelling derived.	(Haq and Lohmann, 1976; Lohmann and Carlson, 1981; Wade and Bown, 2006; Auer et al., 2014, 2019)	Not associated with Mn/Al ratios (= strong OMZ), no strong association with other parameters

1511

Table 2: Interpretation of habitat depth of the identified planktonic foraminifera taxa.

<i>Taxa</i>	<i>Habitat</i>	<i>Reference</i>	<i>Comments</i>
<i>Dentoglobigerina altispira</i>	open ocean mixed-layer	(Berggren et al., 1985; Aze et al., 2011)	Symbiont bearing
<i>Fohsella fohsi</i>	open ocean thermocline	(Aze et al., 2011)	
<i>Fohsella peripheroronda</i>	open ocean thermocline	(Berggren et al., 1985; Aze et al., 2011)	Extends to cool subtropical waters
<i>Globigerina bulloides</i>	upwelling	(Kroon et al., 1991)	
<i>Globigerina</i> sp.	open ocean mixed-layer	(Aze et al., 2011)	
<i>Globigerinita glutinata</i>	open ocean mixed-layer	(Majewski, 2003; Pearson and Wade, 2009)	
<i>Globigerinoides obliquus</i>	open ocean mixed-layer	(Nikolaev et al., 1998)	
<i>Globigerinoides ruber</i>	open ocean mixed-layer	(Nikolaev et al., 1998)	Symbiont bearing
<i>Globigerinoides</i> sp.	open ocean mixed-layer		Based on another present taxa of this genus
<i>Globoquadrina dehiscens</i>	open ocean thermocline	(Pearson and Shackleton, 1995; Nikolaev et al., 1998)	Noted to be erratic and variable by Pearson and Shackleton (1995).
<i>Globorotalia archaeomenardii</i>	open ocean thermocline		Based on similarities to <i>G. manardii</i>
<i>Globorotalia menardii</i>	open ocean thermocline	(Regenberg et al., 2010)	
<i>Globorotalia plesiotumida</i>	open ocean thermocline	(Aze et al., 2011)	
<i>Globorotalia scitula</i>	open ocean sub-thermocline	(Itou et al., 2001)	<i>G. scitula</i> flux is inverse to POC flux
<i>Globorotalia</i> sp.	open ocean thermocline		Based on another present taxa of this genus
<i>Globorotaloides hexagonus</i>	upwelling	(Spezzaferri, 1995)	May also be deep sub-thermocline dweller (Brummer and Kučera, 2022)
<i>Globoturborotalita druryi</i>	open ocean mixed-layer	(Kennett and Srinivasan, 1983; Aze et al., 2011)	Symbiont bearing
<i>Globoturborotalita nepenthes</i>	open ocean mixed-layer	(Aze et al., 2011)	
<i>Neogloboquadrina acostaensis</i>	open ocean thermocline	(Aze et al., 2011)	
<i>Orbulina universa</i>	open ocean mixed-layer	(Aze et al., 2011)	
<i>Paragloborotalia mayeri</i>	open ocean thermocline	(Aze et al., 2011)	
<i>Sphaeroidinellopsis seminulina</i>	open ocean thermocline	(Aze et al., 2011)	
<i>Sphaeroidinellopsis</i> sp.	open ocean thermocline	(Aze et al., 2011)	
<i>Trilobatus quadrilobatus</i>	open ocean mixed-layer	(Chaisson and Ravelo, 1997)	Deep mixed layer in Nikolaev et al. (1998)
<i>Trilobatus sacculifer</i>	open ocean mixed-layer	(Aze et al., 2011)	Symbiont bearing
<i>Trilobatus trilobus</i>	open ocean mixed-layer	(Aze et al., 2011)	Symbiont bearing